# Project 3.16: CT Bridge Girder Sections with Precast Decks and FRP Girder-Deck Shear Connectors

## Final Report
## April 2024

**Principal Investigator:** William Davids Ph.D., P.E.

Department of Civil and Environmental Engineering
University of Maine

**Authors**
Jacob Clark, E.I.
Andrew Schanck, Ph.D., P.E.
William Davids, Ph.D., P.E.

**Sponsored By**
Transportation Infrastructure Durability Center
AIT Bridges

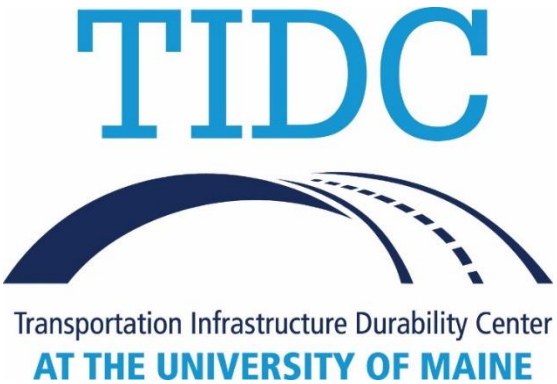


**A report from**
University of Maine
Advanced Structures and Composites Center
35 Flagstaff Road
Orono, ME 04469
Phone: (207) 581-2123
http://composites.umaine.edu

## About the Transportation Infrastructure Durability Center

The Transportation Infrastructure Durability Center (TIDC) is the 2018 US DOT Region 1 (New England) University Transportation Center (UTC) located at the University of Maine Advanced Structures and Composites Center. TIDC's research focuses on efforts to improve the durability and extend the life of transportation infrastructure in New England and beyond through an integrated collaboration of universities, state DOTs, and industry. The TIDC is comprised of six New England universities, the University of Maine (lead), the University of Connecticut, the University of Massachusetts Lowell, the University of Rhode Island, the University of Vermont, and Western New England University.

## U.S. Department of Transportation (US DOT) Disclaimer



## Acknowledgements

Funding for this research is provided by the Transportation Infrastructure Durability Center at the University of Maine under grant 69A3551847101 from the U.S. Department of Transportation's University Transportation Centers Program. [Include any acknowledgements for other contributors (i.e. your university or contributing DOTs/industry partners) here.]

## Technical Report Documentation Page

| | | |
|---|---|---|
| **1. Report No.** | **2. Government Accession No.** | **3. Recipient Catalog No.** |
| **4 Title and Subtitle**<br>Project 3.16: CT Bridge Girder Sections with Precast Decks and FRP Girder-Deck Shear Connectors | | **5 Report Date**<br>**6 Performing Organization Code** |
| **7. Author(s)**<br>Jacob Clark<br>Andrew Schanck<br>William Davids | | **8 Performing Organization Report No.** |
| **9 Performing Organization Name and Address** | | **10 Work Unit No. (TRAIS)**<br>**11 Contract or Grant No.** |
| **12 Sponsoring Agency Name and Address** | | **13 Type of Report and Period Covered**<br>**14 Sponsoring Agency Code** |

**15 Supplementary Notes**

**16 Abstract**

The University of Maine's composite tub (CT) girder, also known as the "GBeam", is a hybrid FRP composite bridge girder system that is a direct replacement for steel and concrete as the main structural members for short-to-medium span bridges. In continuing to develop this technology, this report describes fatigue and strength testing of a novel FRP shear connector and fatigue testing of a full girder section. Shear push-out specimens were subjected to up to 6 million fatigue load cycles and surviving specimens were then subjected to static loading to failure. Of the five specimens, only two were able to withstand the full fatigue loading regiment, and the other three failing prematurely. The surviving specimens displayed reductions in strength up to 35% relative to previously tested specimens with stainless steel shear connectors at much lower stiffness. Two, full-scale CT girder specimens were tested to assess whether bottom flange ply-drops (reductions in the number of layers of fabric reinforcement at a particular, discrete location) are a fatigue critical detail. The first girder was tested in four-point bending to failure in its virgin state to establish base-line strength and stiffness values. Then, a second girder was tested 4-point bending in fatigue for 3 million cycles of high applied load before also being statically tested to failure. After fatiguing, the second specimen retained 67% of the initial girder's strength, indicating damage had occurred. However, the ply-drops did not fail, suggesting that this detail is acceptable if properly fabricated.

| | | | |
|---|---|---|---|
| **17 Key Words**<br>Shear block testing<br>Fatigue<br>CT Girder<br>Fiber Reinforced Polymer | | **18 Distribution Statement**<br>No restrictions. This document is available to the public through | |
| **19 Security Classification (of this report)**<br>Unclassified | **20 Security Classification (of this page)**<br>Unclassified | **21 No. of pages**<br>60 | **22 Price** |

Form DOT F 1700.7 (8-72)

# Contents

## Abstract

The University of Maine's composite tub (CT) girder, also known as the "Gbeam", is a novel, hybrid composite bridge girder system designed with the aim of becoming a one-to- replacement for steel and concrete as the main structural members for short-to-medium span bridges. In continuing to develop this technology, this report describes fatigue and strength testing of a novel FRP shear connector and fatigue testing of a full girder section. Shear push-out specimens were subjected to up to 6 million fatigue load cycles and surviving specimens were then subjected to static loading to failure. Of the five specimens, only two were able to withstand the full fatigue loading regiment, with the other tree failing prematurely. The surviving specimens displayed reductions in strength up to 35% relative to previously tested specimens with stainless steel shear connectors at much lower stiffness. Two, full-scale CT girder specimens were tested to assess whether bottom flange ply-drops (reductions in the number of layers of fabric reinforcement at a particular, discrete location) are a fatigue critical detail. The first girder was tested in four-point bending to failure in its virgin state to establish base-line strength and stiffness values. Then, a second girder was tested 4-point bending in fatigue for 3 million cycles of high applied load before also being statically tested to failure. After fatiguing, the second specimen retained 67% of the initial girder's strength, indicating damage had occurred. However, the ply-drops did not fail, suggesting that these details are permittable.

# Chapter 1: Introduction

## 1.1 Project Motivation and Objectives

The nation's infrastructure is being increasingly relied upon for longer time periods and is being placed under heavier loads. It can be assumed that this trend will continue, requiring reliability to be one of the driving forces in new bridge design and construction. To meet this need for increased durability, the University of Maine is continuing to develop a hybrid fiber reinforced polymer (FRP) composite tub-shaped girder, commercially referred to as the Gbeam, for use as the main structural members of new construction short to medium span bridges. To date, several Gbeam bridges have been constructed or are being constructed in the United States, with others in the planning, design, or construction phases.

With the advent of an all-FRP girder system and the widespread use and acceptance of FRP rebar in reinforced concrete, the possibility of a steel-free bridge using the Gbeam is a possibility. However, to-date, all Gbeam bridges have relied on metallic shear connectors to either maintain composite action with the deck or to prevent uplift between the girders ridged top flange and the deck. In the first portion of this project, five shear block specimens were constructed, tested in fatigue, and then statically tested to failure. These specimens emulated the girder-deck connection but used FRP connectors in place of metallic connectors to investigate their feasibility. The objective of these tests is to ascertain whether FRP shear connectors are a feasible option in their current form.

The behavior and strength properties of the Gbeam are reasonably well-understood when they are new or have been in service for relatively short periods of time. However, with bridge design life increasing, it is imperative that long-term durability be addressed. To better understand the effect of repetitive loading over the course of a bridge's life, two, full-scale Gbeam girders were tested. The first was statically tested to failure soon after its arrival at the University of Maine's Advanced Structures and Composites Center (ASCC) to establish a behavioral baseline. After this, an identical specimen was subjected to 3 million cycles of fatigue loading before being loaded to failure. The objective of these tests is to compare the behavior during failure testing of these two girder specimens to reveal any apparent degradation in flexural behavior and strength over the girder's simulated lifetime.

## 1.2 Report Overview

This report consists of four chapters in addition to this first, introductory chapter:

- Chapter 2 describes fatigue and failure testing of five shear push-out specimens designed to investigate the feasibility of FRP shear connectors in the Gbeam's girder-deck connection
- Chapter 3 describes static failure testing of a virgin Gbeam specimen used as a behavioral baseline for comparison
- Chapter 4 describes the fatigue testing and then static failure testing of a Gbeam specimen to highlight the changes in behavior occurring with repeated loading
- Chapter 5 lists significant conclusions and recommendations for future work

# Chapter 2: Shear Push-Out Testing

## 2.1 Introduction

G-beams are comprised of a FRP tub-shaped girder made composite with an overlying reinforced concrete (RC) deck, which can be cast-in-place, fully precast, or partially precast. Composite action between the FRP and concrete is ensured by a system of sinusoidal ridges cast into the girder top flange, which is in turn imprinted into the concrete, thus providing frictional interlock between the components. Vertical uplift is prevented by shear connectors inserted into the girder top flange and cast into the concrete deck.

One of the major advantages of the G-beam system is the potential for a completely steel-free structure. This would significantly improve durability by eliminating degradation and maintenance due to steel corrosion. To date, steel has been removed from the system-beam superstructures entirely, except for the shear connectors. To economically validate potential shear connectors, shear block specimens were concepted in [1]. A shear block specimen consists of two vertically oriented top flanges facing each other cast against a concrete block two bridge decks thick. An actuator can then apply compressive forces vertically on the cross-sections of the flanges causing a shear force at the interface of the top flanges and the concrete block. This effectively recreates the predominate stresses at shear connectors present in bridges. Figure 2-1 shows a shear block specimen, and additional background on this test design may be found in [2].

Figure 2-1: Shear Block Test

The initial testing of shear blocks led to additional testing of B7 A193 fully threaded rods as shear connectors in [3] and [4] with mixed results. Subsequent testing followed using Grade 8 bolts in [5] which was more successful. It was during this testing when the concept of a sinusoidal ridges first came about. These sinusoidal ridges were then tested in [6], which enabled weaker Grade 5 bolts to be used instead of Grade 8 bolts. Continuing this trend, 18-8 stainless-steel threaded rods were then tested in [7] to improve upon steel's corrosion resistance. Lastly, to

eliminate steel from the structure, further increasing the structure's corrosion resistance, FRP threaded rods and nuts, commercially known as Gbolts, were tested as shear connectors in [8]. However, the conclusions from this study were limited. Further discussion and context for studies [1, 3-6] is given in [2], which covers initial development of shear connectors until the first ridged connectors. Publications [5] and [9] provide further context on the development of shear connectors along with Gbeam testing, with data from studies [6, 7] and [10] respectively.

In this study, five shear block specimens equipped with new Gbar shear connectors were tested to determine their efficacy as shear connectors for Gbeam bridges. The shear blocks were tested in fatigue under AASHTO Fatigue I loading [11] to a maximum of 6-million load cycles, and afterward were statically to failure. As will be seen, only two of the specimens completed fatigue cycling.

## 2.2 Manufacturing

The shear block specimens discussed here used formwork made by the ASCC. Advanced Infrastructure Technologies (AIT) provided vacuum infused top flanges, rebar cages, and Gbar shear connectors. The Gbar shear connectors were 1 in. diameter, hooked FRP rods. They were spaced at 12 in. within drilled holes through the top flanges and clamped in place using two FRP nuts on each side of the flanges. These top flanges, referred to as shear-plates, had sinusoidal ridges with a 0.5 in. amplitude as seen in Figure 2-2.

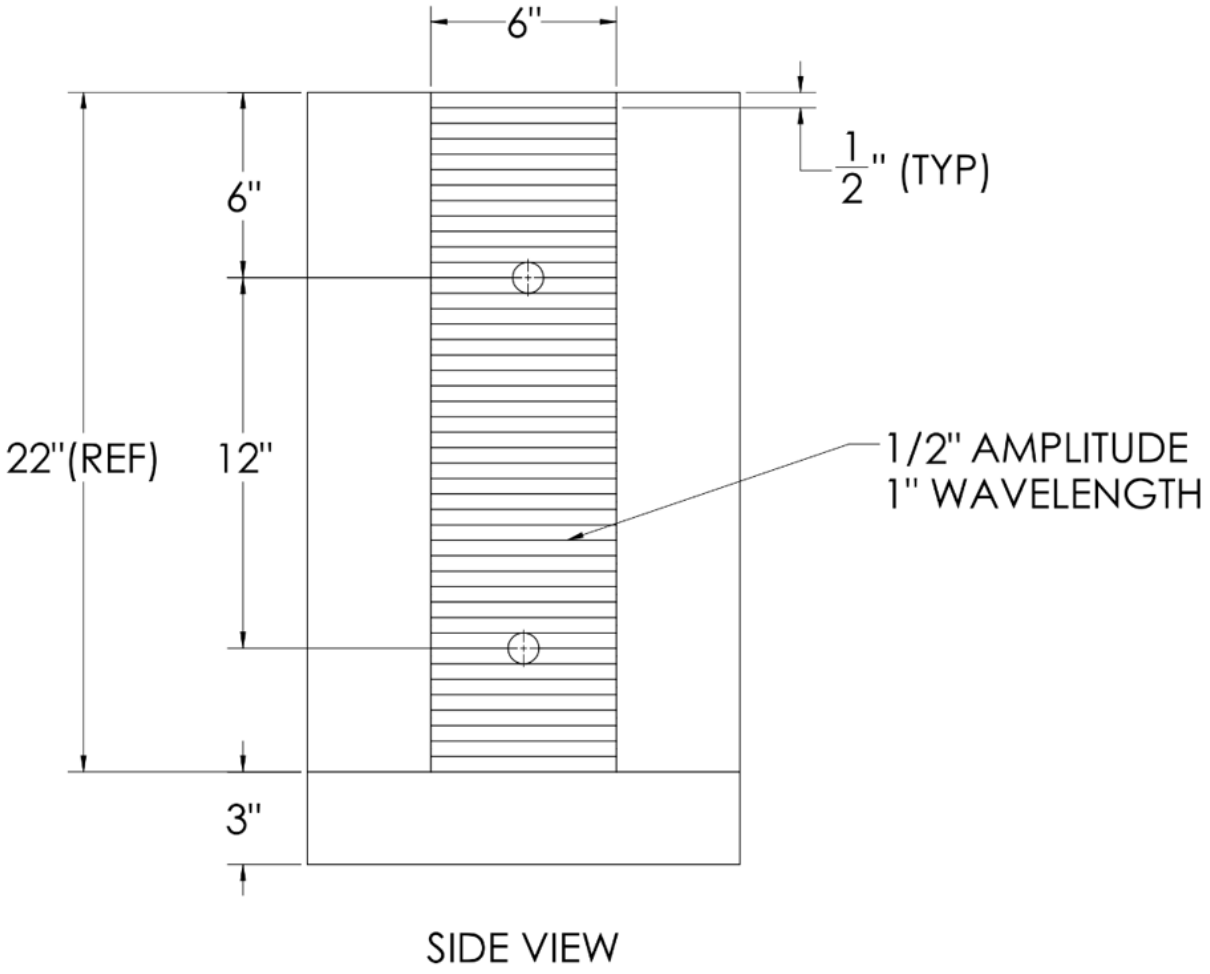


Figure 2-2: Design Drawing of Specimen

Once the FRP plates were cut to final dimension, the specimens were assembled in their molds and all gaps filled with silicone. The shear-plates were arranged such that 22 in. of ridges would be cast into the concrete per shear-plate. The specimens were then sent to American Concrete, a local precaster, for pouring using a standard concrete mix frequently specified by the Maine Department of Transportation for structures. Of the five specimens, three were meant to be tested in fatigue with the remaining two remaining un-fatigued for control. The shear-plates were given the designation code "XY", where "X" denotes the shear block number and "Y" is denoted either A or B to differentiate the plates on either side. Figure 2-3 shows the back side and ridges of plate 1A. Included in Appendix A is the shear-plate ridge quality.

Figure 2-3: Plate 1A Back (Top), Ridges (Bottom)

## 2.3 Fatigue Testing

### 2.3.1 Test Method

Following the previous test method [9], fatigue testing was conducted using the ASCC's 110 kip Instron servo-hydraulic actuator. A steel plate was bolted to the actuator's clevis to load the specimen through the top of the shear-plates and a 1 in. neoprene pad was placed beneath the specimen. This is the set up shown in Figure 2-1.

The specimens were subjected to 6 million load cycles to meet the American Association of State Highway and Transportation Officials' (AASHTO) infinite fatigue life requirement for steel shear studs [12]. Each load cycle was one wavelength of a sinusoidal wave pattern. The troughs and peaks equaled the force required from the actuator to apply the equivalent stresses of a representative bridge's dead and dead plus live loads, respectively to the shear block. The Hampden Twin Bridge project was chosen to provide representative loadings as it was used in the last generation of shear block testing [9]. This resulted in an approximate fatigue range of 29 – 71 kips, which was applied at a rate of 4 Hz. These loads were calculated using ASSHTO Fatigue I loading [11] and are included in Appendix B.

Load, displacement, and slip data were recorded throughout the duration of fatigue testing. Load and displacement data were collected by the Instron's internal load cell and linear variable differential transformer (LDVT) respectively, while slip data were measured between the shear-plates and concrete block using inductive linear position sensors. The inductive linear position sensors are an upgrade over the previously used LVDTs [8] due to their improved fatigue life. These sensors were mounted in aluminum brackets adhered to the shear-plates and to the concrete Each side of the specimen was equipped with two sensors, one adjacent to the top shear connector and one adjacent to the opposite side of the bottom shear connector, as shown in Figure 2-4.

Figure 2-4: Linear Position Sensor (Left); Test Setup (Right)

In addition to the fatigue loading, static stiffness tests were also performed on the specimens automatically to monitor any degradation of stiffness. These tests were conducted intermittently at 0, 1,000, 10,000, 100,000, 200,000, 500,000 cycles, and every subsequent 500,000 cycles after. During each stiffness test the shear block was unloaded to 4 kip, slowly loaded to the peak fatigue load of 71 kip, then unloaded to 4 kip before returning to the wave midpoint and resuming fatigue loading.

### 2.3.2 Fatigue Testing Overview

Since there were several different outcomes and the shear blocks were not tested sequentially, Table 2-1 is included to give an overview of each shear block tested. Only one of the initial fatigue specimens, shear block 2, completed fatigue testing. Shear blocks 1 and 3 failed before completing 6 million fatigue cycles. Failure meant the shear block had accumulated damage that prevented the shear transfer through the sinusoidal ridges. As a result, both control specimens were fatigued as well to see if they would also fail prematurely. One of the control specimens completed fatigue testing and the other failed prematurely. As can been seen in Table 2-1, the failures during fatigue testing do not necessarily prove or disprove the efficacy of the shear blocks tested due to obfuscating factors.

Table 2-1: Testing Overview

| Specimen | Start Date: | End Date: | Notes: |
|---|---|---|---|
| 1 | 03.08.22 | 03.10.22 | Failed at 368 thousand cycles, missing cross brace |
| 2 | 02.08.22 | 02.27.22 | Completed 6 million cycles |
| 3 | 01.13.22 | 01.18.22 | Crushed by Instron at 1.4 million cycles |
| 4 | 03.15.22 | 04.05.22 | Completed 6 million cycles |
| 5 | 04.06.22 | 05.21.22 | Paused at 2.8 million cycles on 04.14.22, resumed testing 05.16.22 and failed at 4.5 million cycles |

The results of the periodic stiffness tests performed during fatigue testing are shown in Figure 2-5. To measure the connection stiffness, the displacement values used are the average slip values measured by the sensors against the starting displacements of the stiffness test. This is unlike the accumulated slip values used elsewhere where the slip is relative to the initial displacements of fatigue cycle 1. A linear-least squares fit of the load-slip curve was used to determine the slope of the periodic stiffness test curves, and therefore the periodic stiffnesses.

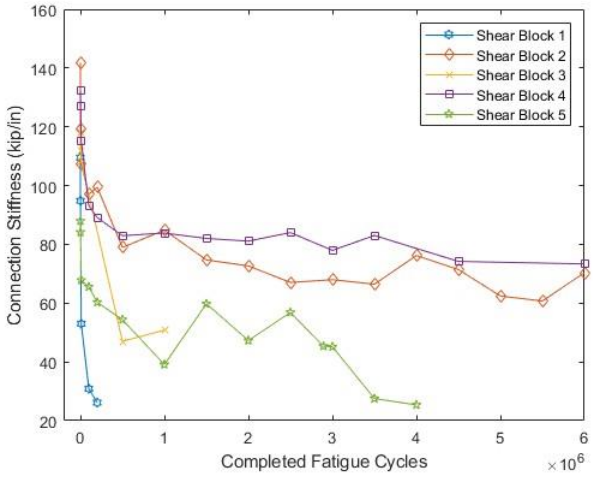


Figure 2-5: Stiffness Testing

Throughout the duration of shear block testing, intermittent concrete cylinder compression testing was conducted. These tests are necessary as the strength of the concrete ridges is related to that of the concrete [8]. The results of this testing are shown in Appendix A. Due to a limitation of 13 concrete cylinders, compression tests were conducted during strength testing and at the start of alternating fatigue tests. Tests were performed at the ASCC in accordance with [12].

### 2.3.3 Shear Block 1 Results and Discussion

Shear Block 1 completed 368,000 cycles before prematurely failing due to a loss of composite action between the shear-plate and concrete block. This is shown by the visible gap in the connection in Figure 2-6. An inspection of the failed side with the shear-plate removed is shown in Figure 2-7. This inspection revealed that the concrete ridges had sheared off, the top shear connector had splintered apart, and the bottom nut had cracked, further showing the effects of a failure.

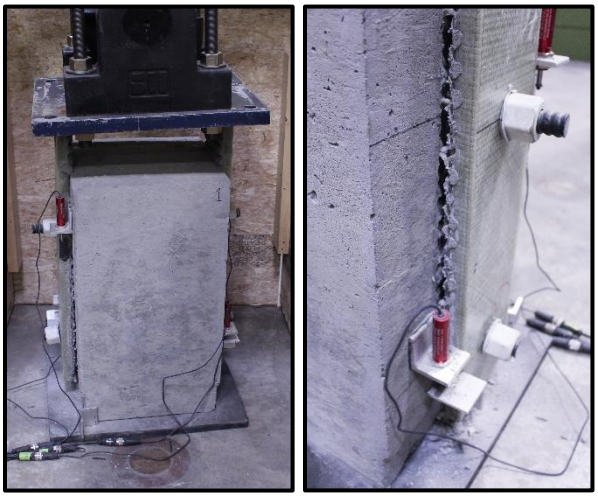

Figure 2-6: Shear Block 1 Failure

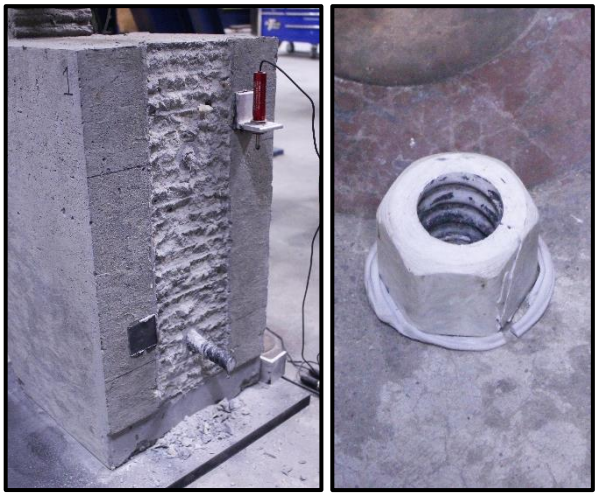

Figure 2-7: Shear Block 1 Failure Inspection

Figure 2-8 shows the accumulated slip of the shear connection at each fatigue cycle. Accumulated slip is the difference in initial slip between each load cycle and the first load cycle. Slip is the relative displacement of the shear-plate to the concrete block. Therefore, increasing accumulated slip values means the shear-plate is displacing relative to the concrete block because of each cycle, and is not an indication of intracycle slip increasing. Constant slip values indicate the connection is enduring the applied loads. Figure 2-8 shows the failed shear-plate's accumulated slip increasing throughout testing with rapid increases around 75,000 and 350,000

cycles. Shown in Appendix A are the slips as a function of load at the start and end of fatigue testing.

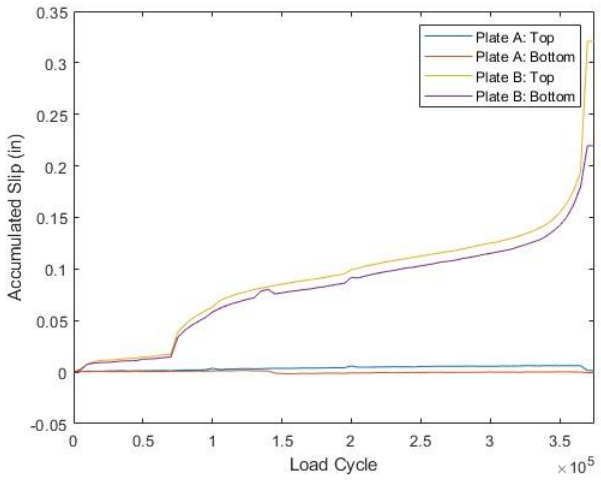


Figure 2-8: Shear Block 1 Accumulated Slip Vs Load

The rapid increases of accumulated slip in Figure 2-8 suggest damage occurring, as opposed to gradual increases indicating general wear in the connection. As it will be seen with future shear blocks, the first increase in slip to 0.01 in. is nearly double the maximum slip of the shear blocks that completed fatigue testing. This may have been caused by the FRP nut cracking since the nut restrains the plate from moving but does not carry the shear loads. Therefore, it could incur damage resulting in an increase in slip without the shear block completely failing. Furthermore, it likely is not a result of the concrete ridges shearing, as they are better explained by the second exponential increase in slip. Assuming the shear-plate was no longer restrained as intended, the ridges between the shear-plate and concrete had opportunity for partial contact. This may have deteriorated the ridges, sequentially shearing them off faster as less were available to carry the fatigue loads.

A probable root cause for the premature failure is a missing cross brace between the shear-plates of shear block 1. The cross brace is a steel threaded rod that is intended to prevent unintended eccentric loads from horizontally loading the shear-plates, causing the shear-plates to pry on the other shear connection elements. This prying could fatigue load these components in a way they were not designed for. Figure 2-9 shows a shear block with a cross brace and shear block 1 without its cross brace. Lastly, the low ridge quality of shear block 1, given in Appendix A, may have contributed to the premature failure by further reducing the contact of the ridges.

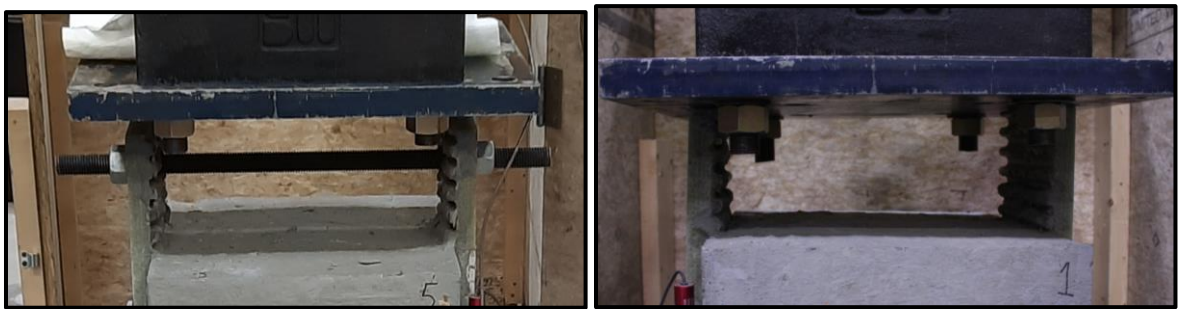

Figure 2-9: Shear Block with a Cross-Brace (Left); Shear Block 1 Without a Cross-Brace (Right)

### 2.3.4 Shear Block 2 Results and Discussion

Shear block 2 completed its six million fatigue cycles without failing. Figure shows the accumulated slip as a function of load cycle. The accumulated slip increasing indicates the connection displaced from its initial position at the start of fatigue testing. An initial increase during the first million cycles, followed by a gradual increase, as shown in Figure 2-10 are typical of previous shear block testing. However, the negative slips in the bottom of plate A are not expected behavior. A negative slip indicates the linear position sensor read smaller displacements over the course of testing.

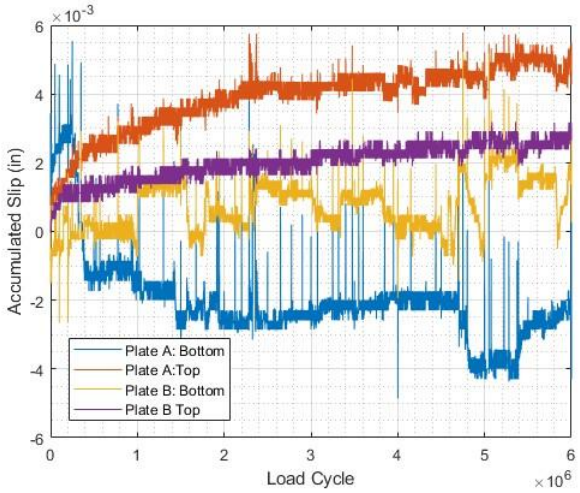


Figure 2-10: Shear block 2 Accumulated Slip Vs Load Cycle

Figure 2-11 presents the average slip from the four sensors recorded during the 1,000$^{th}$ and 6,000,000$^{th}$ load cycles, showing the effects of load and duration on the recorded slip. The horizontal shift from left to right from the curve at 1,000 cycles to 6,000,000 shows the accumulation of permeant slip during testing. A clockwise rotation in the later curve indicates a decrease in the connection's stiffness, leading to a larger slip at the same load. Lastly, it can be observed from the minimal difference between the loading and unloading branches that there is little hysteresis in the system in either load cycle. This implies that only a small amount of intracycle damage was accumulated.

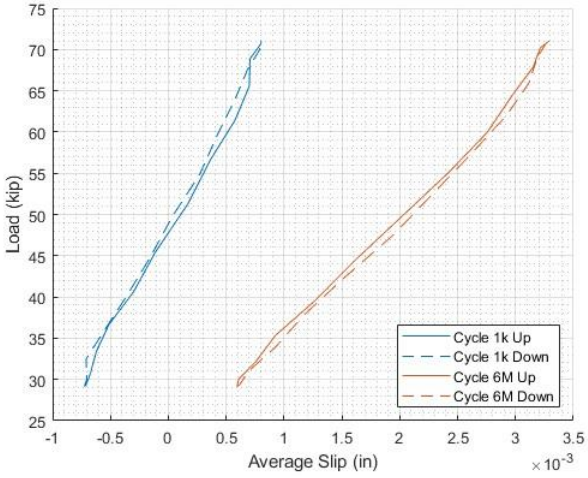


Figure 2-11: Shear Block 2 Average Slip Vs Load

The sensor at the bottom of Plate A initially has the largest positive slip before rapidly transitioning to a negative slip as can be seen in Figure. If both sensors on the same side read negative, a rotation of the shear-plates about the concrete block may have occurred, however that is not the case here. In this case the positive start and ending accumulated slip-load cycle slopes, along with the large negative slip accumulation around 500,000 cycles, may indicate the sensor "settled" during the start of testing.

### 2.3.5 Shear Block 3 Results and Discussion

Shear block 3 completed 1.4 million cycles before it prematurely failed, likely due to an unexpected load spike from the actuator. Failure occurred on the side of shear-plate B as shown in Figure 2-12. Figure 2-13 shows shear-plate B's failed shear connectors, concrete ridges, and a bend in shear-plate A. Unlike in other failures, the bottom FRP nut also was found on the ground apart from the shear block.

Figure 2-12: Shear Block 3 Premature Failure

Figure 2-13: Failed Side (Left); Cracked Nut (Center); Bent Shear-Plate A (Right)

Figure 2-14 shows the accumulated slip as a function of load cycle for shear block 3. Increase in accumulated slip indicate displacement in the connection relative to its initial position. The flat lines in the data are a result of missing or corrupted data. During the missing data cycles, the accumulated slip appears to gradually increase as expected. After the missing data ends, the slips recorded in plate A remain relatively constant while plate B continues to increase. The erratic jumps in slip recorded at the bottom of plate B appear to be random, indicating the data from the bottom of plate B may be false readings.

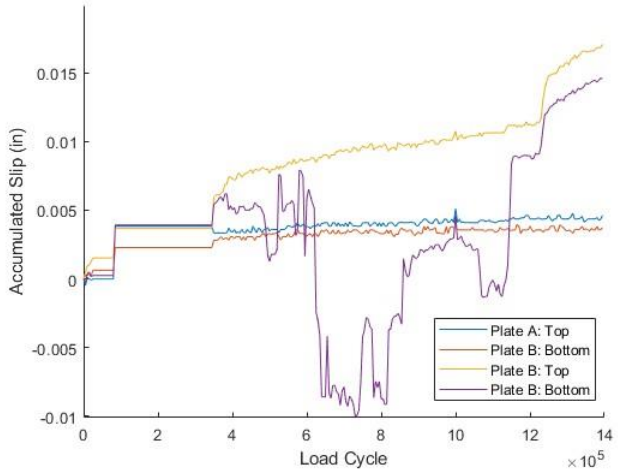


Figure 2-14: Shear Block 3 Accumulated Slip Vs Load Cycle

Shear block 3 likely failed due to a load spike caused by a malfunction of the Instron controller. Despite the premature failure however, it is possible that the shear block would have failed prematurely during fatigue testing. Both the accumulated slip and stiffness of shear block 3 exceeded those of the specimens that completed 6 million fatigue cycles. Figure 2-114 shows the accumulated slip in shear-plate B near failure reached 0.015 in., three time that of shear block 2. Additionally, the stiffness of shear block 3 was already half that of shear blocks 2 and 4 at one million fatigue cycles as shown in Figure 2-5. Notably, a bend occurred in shear-plate A, which is unique to this shear block. This may be a result of combined bending and buckling in the plate. As plate B failed, the cross braced was pulled with it, applying a lateral bending force on plate A. Additionally, as the plate bent it was compressed as well, increasing the moment, and potentially buckling the plate as well.

### 2.3.6 Shear Block 4 Results and Discussion

Shear block 4 completed six million fatigue cycles. Figure 2-15 shows the accumulated slips of the shear block as a function of completed cycles, where increases in accumulated slips indicate an increase in displacement between shear-plates and concrete. This shear block has several locations of corrupt data shown as flat lines. The sensor corresponding to the top of shear-plate A spikes in magnitude several times. Due to spikes in slip from the sensor at the top of plate A, the Y-axis of the plot has been cropped to better show the magnitudes of the remaining sensors' slip data.

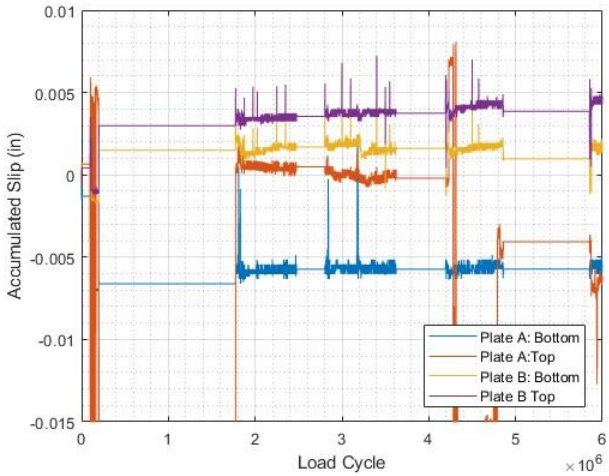

Figure 2-15: Shear Block 4 Slip Data

Figure 2-16 shows the load-slip response of shear block 4 at 1,000 and 6,000,000 completed fatigue cycles. Since the sensor corresponding to plate A's top had noticeably larger magnitudes than the other sensors, and displayed erratic data trends, it was removed from the calculated average slip. The figure shows how the load-slip response of the shear block changed over the course of testing. This reveals accumulated slip through a horizontal shift in the curve, and a decrease in stiffness through a clockwise rotation.

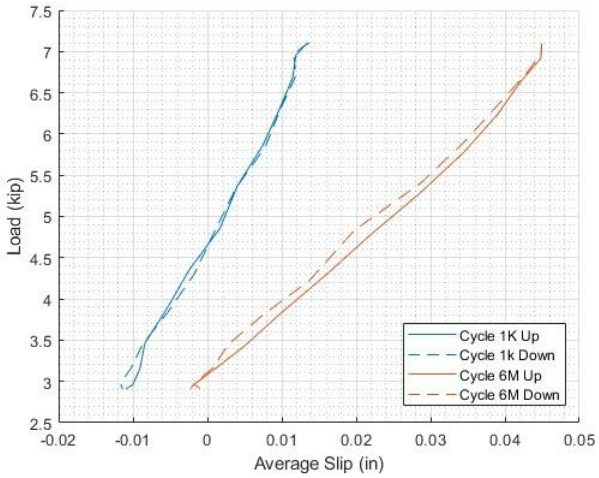

Figure 2-16: Shear Block 4 Average Slip Vs Load

The slip recorded by the sensor corresponding with plate A's top spiked in magnitude several times throughout fatigue testing. Since the other sensors did not record similar behavior, it is likely that unusable data was produced by the sensor. Therefore, this sensor was ignored when calculating the stiffness presented in Figure and the average slips presented in Figure 2-16. Much of the recorded data were corrupt, as seen by the horizontal lines in Figure 2-15. However, shear block 4 still shares the trends and magnitudes of accumulated and average slip with shear block 2 which also completed fatigue testing.

### 2.3.7 Shear Block 5 Results and Discussion

Shear block 5 completed 4.5 million cycles before the side of plate B unexpectedly failed as shown in Figure 2-17. Like shear blocks 1 and 3, the concrete ridges, bottom FRP nut, and Gbar shear connector had failed. Figure 2-18 shows the accumulated slips between the shear-plate and concrete block of the shear block over the test duration. These accumulated slips remained relatively constant for the first three million load cycles. After this, the slip in plate B began to increase rapidly, failing with 0.1 in. of accumulated slip. Figure 2-19 shows the average slip-load response of the shear block at 1,000 cycles and at 4.5 million complete cycles. Since the horizontal displacement between the curves is the difference in accumulated slip between the two cycles, the X-axis scale is relatively large for showing the slips within each load cycle. Additionally, the distance between these two curves is about 0.055 in. and not 0.1 in. since these curves average the slips of both sides of the shear block together.

Figure 2-17: Failed Shear Block 5

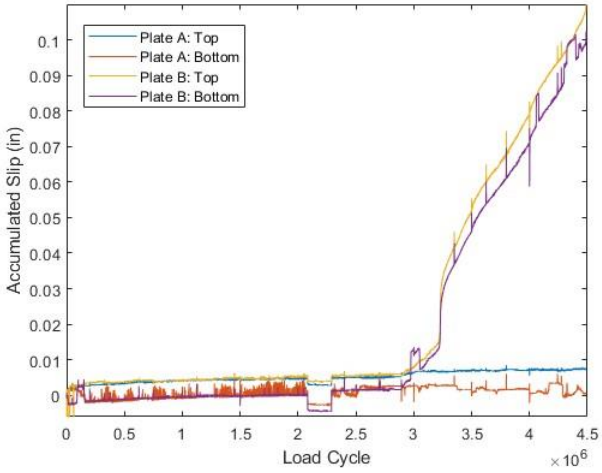


Figure 2-18: Shear Block 5 Accumulated Slip Vs Load Cycle

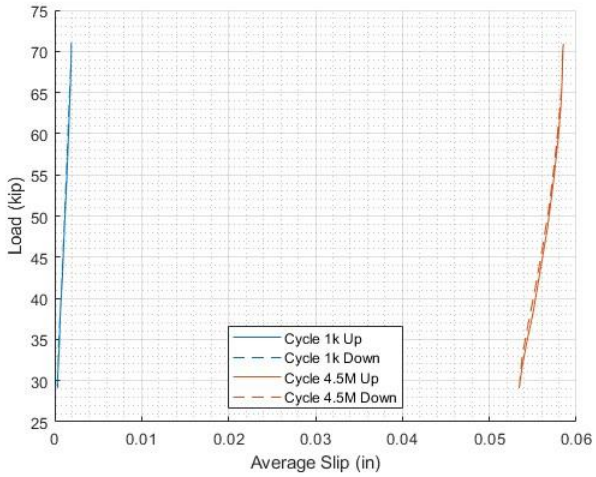

Figure 2-19: Shear Block 5 Average Slip Vs Load

Fatigue testing of shear block 5 was paused for four weeks during actuator maintenance after nearly 2.9 million fatigue cycles had been applied. During this time care was taken to minimize disturbance to the specimen, although it needed to be removed from the load frame to prevent damage. After completion of maintenance and restarting the test, block 5 failed around 1.7 million additional fatigue cycles later. When fatigue testing of shear block 5 resumed the accumulated slip in Figure 2-1 increased and the stiffness in Figure 2-5 decreased. This correlation suggests that the specimen's premature failure may have been impacted by the pause in testing, despite of the care implemented to minimize disturbance to the block during this pause. It is possible that the specimen could have been inappropriately moved or struck, causing damage. However, such damage is not likely considering no damage has occurred to date because of movement. Furthermore, an invasive procedure has previously been performed to remove shear-plates from shear blocks prior to testing in [7] without causing any issues. Therefore, it cannot be concluded that damage incurred during the pause caused a premature failure.

### 2.3.8 Conclusions from Fatigue Testing

The results of fatigue testing were somewhat obfuscated due to a series of unforeseen variables. Shear block 1 most likely failed due to a missing cross brace, shear block 3 was likely crushed due to an actuator malfunction, and shear block 5 failed unexpectedly after a four-week testing pause. However, insights can still be made from shear blocks 3 and 5. Shear block 5 had been clearly labeled to not be disturbed with contact information, and the stiffness before and after the testing pause shown in Figure 2-5 around three million cycles is almost identical. Unless a major incident occurred with shear block 5 during its testing pause which was both unobserved, and unreported, it mostly likely failed purely from fatigue testing. Shear block 3 had accumulated slips and decreasing cycle stiffness prior to being crushed by the actuator like shear blocks 1 and 5 prior to their failures mid fatigue testing. Since these trends are unique to the shear blocks that failed during fatigue testing, it is likely shear block 3 would have failed during fatigue testing as well. Therefore, the shear connectors used in this study were inconsistently adequate in fatigue to complete six million fatigue cycles under the Hampden Twin Bridge project loading.

Comparing the tested shear block stiffness with previous testing provides additional insight. The connection stiffness of shear blocks using G-bar shear connectors was lower than those reported in previous studies. Reference [9] reported an average stiffness of 3,570 kip/in. using pretensioned grade 8 bolts. Reference [10] reported an average stiffness of 24,300 kip/in. using pretensioned grade 5 bolts and sinusoidal plates, and reference [8] had the lowest average stiffness of 419 kip/in. The average stiffness in this study is the lowest at 71.8 kip/in. from the blocks that completed fatigue testing. If the stiffness of shear blocks 3 and 5 were included before any aberrations occurred, this value would be in even lower. While it is unclear how much stiffness is required for effective composite action, since [9] is the lowest stiffness connection that has been demonstrated, it is clear that the tested shear connectors were the most compliant shear connectors tested to date. Therefore, this may result in larger strains and stresses in a Gbeam system if implemented. Furthermore, this trend correlates with bolt pretension. Tests in reference [9] had a bolt pretension of 50 ft-lbs, tests in reference [10] reported 225 ft-lbs, and the present study and reference [8] were hand tight. By using data from the shear blocks that prematurely failed, and those from previous studies, it is possible to conclude that the shear connectors tested here did not perform well in fatigue. However, additional fatiguing testing is required to definitively confirm the high failure rate of shear blocks in this study was not an anomaly.

## 2.4 Strength Testing

A shear connector needs to meet both AASHTO's [11] fatigue life and Strength-I requirements to be viable in bridge design. Strength-I loading is the maximum factored vehicular loading that the AASHTO design code requires of bridges. Therefore, upon fatigue testing completion the shear blocks were then strength tested to failure to verify their strength.

### 2.4.1 Specimen Preparation

A discussion with AIT Bridges led to the decision to apply a slight tensioning to the GBar shear connectors following the completion of fatigue testing. To prevent tension from being released, epoxy also needed to be applied to the nuts to prevent them from backing off. To apply epoxy to the GBar shear connectors the FRP nuts were first unthreaded using a wrench to overcome adhesive action for the silicone that was bonding the two pieces together. The existing silicone was then scraped off and both the nut and Gbar lightly roughened with sandpaper and cleaned with denatured alcohol as surface preparation for bonding. Scotch-Weld DP110 Translucent 2-Part Epoxy Adhesive was then applied to the Gbar shear connectors, and the nuts were then snug-tightened by hand. Once snugged, the nut position was marked and tightened an additional approximate 1/8$^{th}$ turn. This process can be seen in Figure 2-20.

Figure 2-20: Applying Epoxy to the Shear Blocks

### 2.4.2 Test Method

The shear blocks were strength tested using the ASCC's 300 kip servo-hydraulic Instron actuator. Specimens were placed on a neoprene pad and loaded through a steel plate bolted to the load head of the actuator. Prior to strength testing, the specimens were ramp-loaded in three minutes to the peak fatigue load and unloaded three times to provide additional data on the connection stiffness. The specimens were then loaded in displacement control until they were deemed failed by the lead engineer present due to significant and continuing drops in load with increasing enforced displacement. Load and displacement data were recorded using the 300 kip Instron's load cell and internal LDVT. Figure 2-21, shows a prepared specimen prior to testing.

Figure 2-21: Failure Test Setup

### 2.4.3 Strength Testing Overview

Having completed six million fatigue cycles to meet AASHTO's [11] infinite fatigue life requirements, shear blocks 2 and 4 were strength tested to see if they would meet AASHTO's Strength-I requirements as well. This was accomplished by comparing the shear flow at failure of the shear bocks tested against the shear flows present during Strength-I loading of the Hampden Twin Bridge project. A shear-flow is in units of shear force per length and is typically used in the design process of shear connectors for bridges. The Hampden Twin Bridge project was chosen to stay consistent with fatigue loading and the previous shear block study [8]. Corresponding shear flow calculations are provided in Appendix B. The resulting Strength-I shear flow and calculated maximum shear flows from strength testing are shown in Table 2-2. Note that the shear flow at failure is not the same thing as the design shear flow capacity of the shear connectors, which is less than the shear connector's ultimate strength due to the application of a strength reduction factor. The corresponding failure loads of shear blocks 2 and 4 are 111 kip and 121 kip respectively. It is important to note that these strengths are significantly less than the average strength of 171 kip from post-fatigue strength tests of nominally identical specimens with stainless steel connectors reported in [10].

Table 2-2: Strength Testing Results

| Shear Block | Failure Shear Flow (kips/in.) | Strength-I Shear Flow (kips/in.) |
|---|---|---|
| 2 | 2.52 | 2.49 |
| 4 | 2.75 | 2.49 |

Figure 2-22 shows the force displacement data recorded from the Instron during the strength testing of shear blocks 2 and 4. The curves are approximately linear until the first load drop, indicating elastic deformation in the shear blocks. After the peak, the load plateaus before rapidly dropping, and the failure was generally brittle.

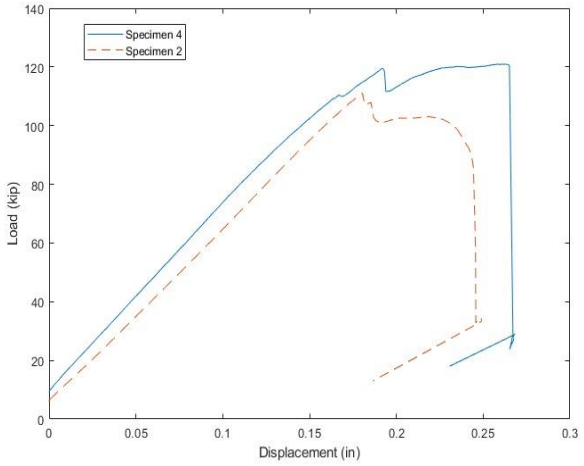


Figure 2-22: Strength Testing

The stiffnesses of the shear blocks were also calculated from the three stiffness loadings and the strength testing loading using a linear least-squares fit of the load-slip curves. These values along with the stiffness of the shear blocks upon their completion of fatigue testing are shown in Table 2-3.

Table 2-3: Connection Stiffness During Strength Testing

| Shear Block | Fatigue Completion (kip/in) | Stiffness 1 (kip/in) | Stiffness 2 (kip/in) | Stiffness 3 (kip/in) | Strength (kip/in.) |
|---|---|---|---|---|---|
| 2 | 70.35 | 10,700 | 10,800 | 11,100 | 10,200 |
| 4 | 73.34 | 12,900 | 12,800 | 12,800 | 12,400 |

### 2.4.4 Shear Block 2 Strength and Stiffness Testing

Figure 2-23 shows the resulting load-slip plot for shear block 2. The slip data are an average of the slip in each of the four DIC marker pairs. The corresponding load-slips curves behaved linearly while loading, but form "humps" while unloading. These may be a result of the actuator overshooting the intended loading, requiring operator intervention to manually unload the shear block each time. This is unexpected as shear block 2 was tested using the same programming that stiffness and strength tested shear block 4 already. Lastly, the figure shows that plate A has a lower stiffness then Plate B. This matches the general slip trends between Plate A and Plate B previously shown in Figure 2-10.

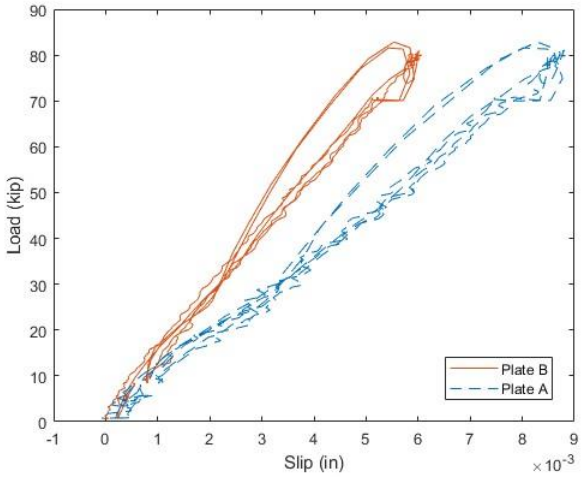


Figure 2-23: Shear Block 2 Pre-Failure Stiffness Testing

Plate A, the lower stiffness side, is also the side that ultimately failed during testing. Figure 2-24 shows the actuator load corresponding to the slips recorded between each shear-plate and the concrete block. The data in the plot has been cropped down to better show the slips leading up to failure, while Figure 2-2 shows the original data. In this figure Plate A appears to continue carrying diminishing amounts of load as permeant slip increases. However, this is not a ductile failure as previously discussed with Figure 2-22. Instead, Figure 2-2 shows that Plate B continued to carry load while Plate A failed. This is a result of the actuator measuring the gross load being resisted by shear block, and then that data being plotted against the slips in both plates irrespective of how much each plate contributes to resisting the load. Also, Plate B did not fail with Plate A because the actuator load head rotated away from Plate B.

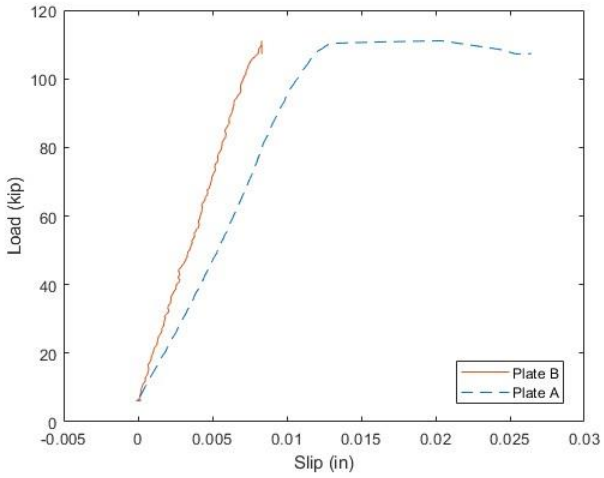


Figure 2-24: Shear Block 2 Failure

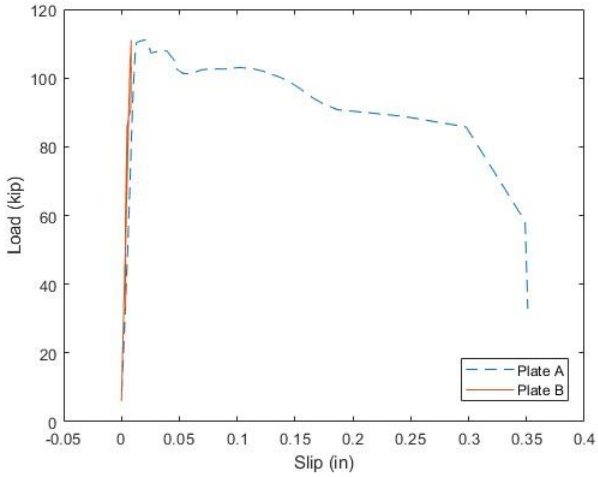


Figure 2-25: Shear Block 2 Complete Failure Curve

During the failure of shear block 2, there was a large and a small load peak, followed by a plateau proceeding failure in Figure 2-2. To determine the corresponding failure sequence of the shear connection, the protos presented in Figures 2-26 and 2-27 were taken. Figure 2-26 shows the shear block post failure. Plate A was removed to examine the extent of the damage, revealing the concrete ridges had sheared off the specimen, and both FRP nuts had cracked. The Gbar however, had not failed in shear. Meanwhile, Figure 2-27 shows crack propagation through the bottom FRP nut as it split apart. These images correspond to the transition between the plateau in Figure 2-22, and the rapid load drop afterwards. From these images it is most likely that failure started with the concrete ridges at peak load. Then, the shear connectors began to bend as they carried more of the shear load. This caused the shear-plates to push against the FRP nuts, which then cracked under the loading. This allowed the shear-plate to then slide along the shear connector, unloading it.

Figure 2-26: Shear Block 2 Failure

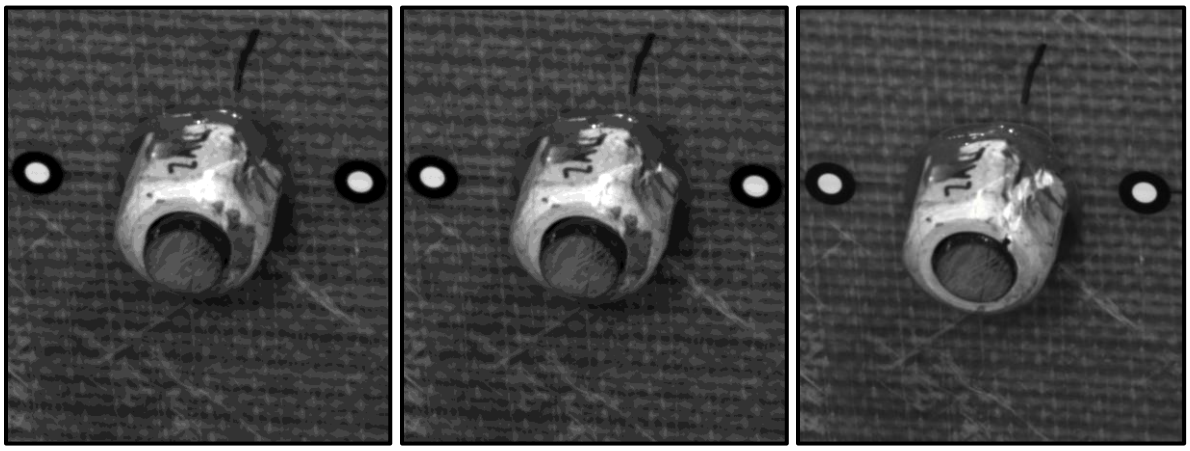

Figure 2-27: Shear Block 2 DIC Progressive Nut Failure

### 2.4.5. Shear Block 4 Strength and Stiffness Testing

Figure 2-28 shows the load-slip curves for each shear-plate on shear block 4. The slip is an average of the slips measured by Digital Image Correlation (DIC). The figure shows loading and unloading curves behaved approximately parallel and linearly. There is a small offset between the loading and unloading paths which may be a result of the neoprene bearing pad settling during a five second pause at the peak load and relaxing during a five second pause at the minimum load. Plate A was stiffer than Plate B, but the difference in stiffness between the two sides is much less than the difference in the two sides observed in shear block 2.

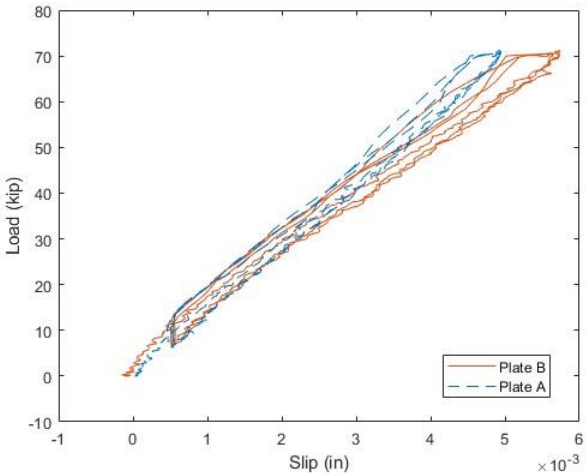

Figure 2-28: Shear Block 4 Pre-failure Stiffness Testing

Figure 2-29 shows the load-slip relationship of shear block 4 during strength testing. This plot has also been cropped to better show the relative slips between the two shear-plates. However, the second load peak shown in Figure 2-2 is marginally higher than the first which Figure 2-29 is cropped to. Therefore, the slips relating to Plate B are cut off. The shear block was approximately linear to begin but gradually softened nearing the peak loads. Shear Plate B, the less stiff side, had an initial loss in stiffness while carrying load before failing once the shear block reached its second peak load. Shear block 4 sustained higher loads than shear block 2 before failing.

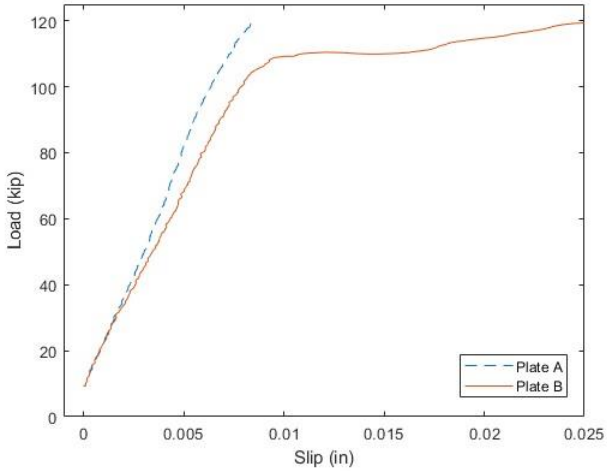

Figure 2-29: Shear Block 4 Failure

The effects of failure on shear block 4 are like those observed in shear block 2. Figure 2-30 shows the concrete ridges failed, and the G-bar shear connectors did not. The FRP nuts are cracked as well. Figure 2-3 shows the DIC frames corresponding to before and after the first load-displacement peak seen in Figure 2-2. In Figure 2-31 a crack forms in the concrete to the right of the shear-plate along its bottom edge, and a crack to the left expands, spalling concrete off. Figure 2-32 shows the DIC frames corresponding to the second load-displacement peak. In these frames the previous cracks expand and release from the stud, and the FRP nuts crack apart.

Both sets of DIC frame suggest the concrete ridges initially failed or started failing during the first load peak, leaving the shear connectors to carry the load until the FRP nuts failed during the second and final load peak.

Figure 2-30: Shear Block 4 Inspection

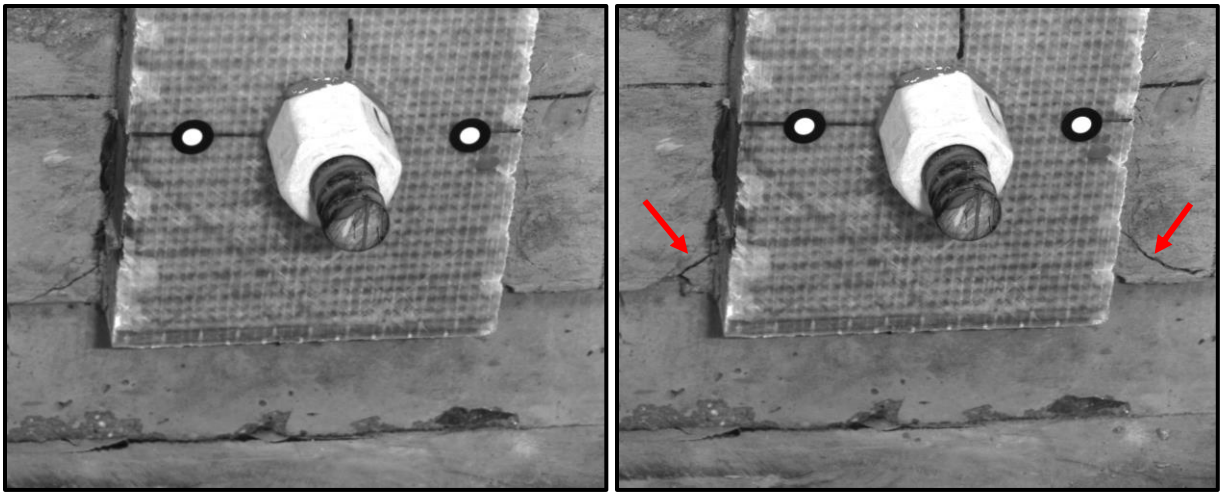

Figure 2-31: Shear Block 4 DIC Frames Before and After the First Load-Displacement Peak

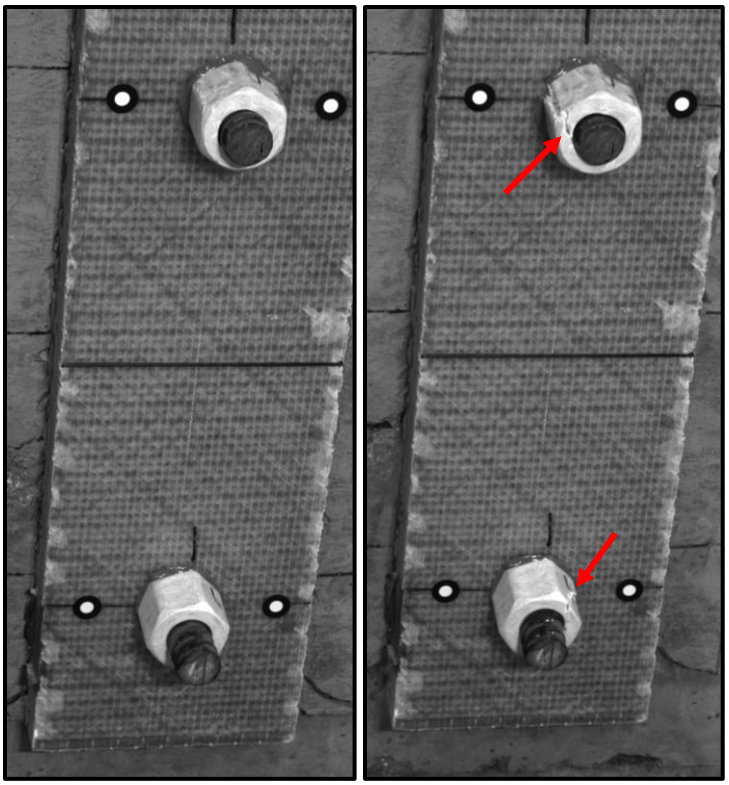

Figure 2-32: Shear Block 4 DIC Frames Before and After the Second Load-Displacement Peak

### 2.4.6 Conclusions from Strength Testing

An unexpected result of stiffness testing the shear blocks prior to strength testing was their two orders of magnitude increase in stiffness. The shear blocks increased from an average stiffness of 71.85 kip/in. to 11,700 kip/in. This is most likely a result of the epoxy applied to the shear connectors before strength testing, as nothing else about the shear blocks were changed between fatigue testing and strength testing. Since the epoxy was added after fatigue testing however, additional fatigue testing with the epoxy is required to ensure this increase is stiffness does not significantly diminish with load cycles.

While both shear block specimens exhibited strength close to the Strength-I demand corresponding to the Hampden Twin Bridge, the specimens exhibited 30%-35% less strength than similar specimens fabricated with the stainless-steel connectors that are currently used in practice. While concrete ridge shear failure was observed in the specimens tested here, the FRP nuts in this study also failed in every test. This suggests the FRP nuts are not strong enough to allow the development of tension in the FRP connector that is required to confine the concrete ridges and delay their failure.

# Chapter 3: Full-Scale CT Girder Strength Testing

## 3.1 Introduction

Including its debut test in 2018, four CT (Gbeam) girders have been previously tested with various levels of success [9], but only one CT girder has been subjected to full flexural failure. However, this test was of a pilot specimen, and significant changes have been made to both the girder-deck shear connectors as well as the girder cross-section since that initial girder. Further, to-date no girder has been subjected to fatigue loading to assess residual fatigue capacity. Assessment of residual fatigue strength is especially important in light of the use of ply drops in the bottom flange to reduce the amount of unidirectional carbon fiber in regions of lower moment. To address the lack of full-scale girder test data, two new CT girders, designated "UTC-3" and "UTC-4" were manufactured by AIT Bridges for testing by the ASCC. UTC-3 was tested statically under increasing load up to failure. The results of this testing were also used as a control to compare with UTC-4, which would be statically tested to failure after fatigue testing.

## 3.2 Test Details

### 3.2.1 Specimen Design

Specimens UTC-3 and UTC-4 were designed to be nominally identical, with similar geometric and laminate properties. These were taken to emulate a single, interior girder from the recently constructed Cottrell Bridge in Westerly, Rhode Island. One notable deviation from the Cottrell Bridge was the inclusion of ply drops in the bottom flange, which have been used in other structures. These ply drops are locations in which the number of carbon layers within the bottom flange are reduced, helping to reduce the girders' overall cost. Table 3-1 lists the location of ply drops, as well as the number of carbon plies contained in each zone. To prevent shear failure at the girder ends, additional 3-D woven E-glass plies were added to the webs of the girders in Zone 1. The precast concrete deck was designed with a nominal compressive strength of 5.0 ksi and was made composite with the girder by grouting. This grout formed around the ridges in the girder's upper flange providing adequate shear interlock [10].

Table 3-1: Bottom Flange Ply Drops

| Zone | Zone 1 | Zone 2 | Zone 3 | Zone 2 | Zone 1 |
|---|---|---|---|---|---|
| Location | 0ft – 4ft | 4ft – 8ft | 8ft – 30ft | 30ft – 35ft | 35ft – 38ft |
| Number of Carbon Layers | 1 | 2 | 4 | 2 | 1 |

### 3.2.2 Set-Up and Instrumentation

UTC-3 was set up in a 4-point bend configuration beneath the 300 kip load frame in the ASCC's Offshore Wind Lab (OWL). This can be seen in Figures 3-1 and 3-2, which show the girder from a back and side elevation view, respectively.

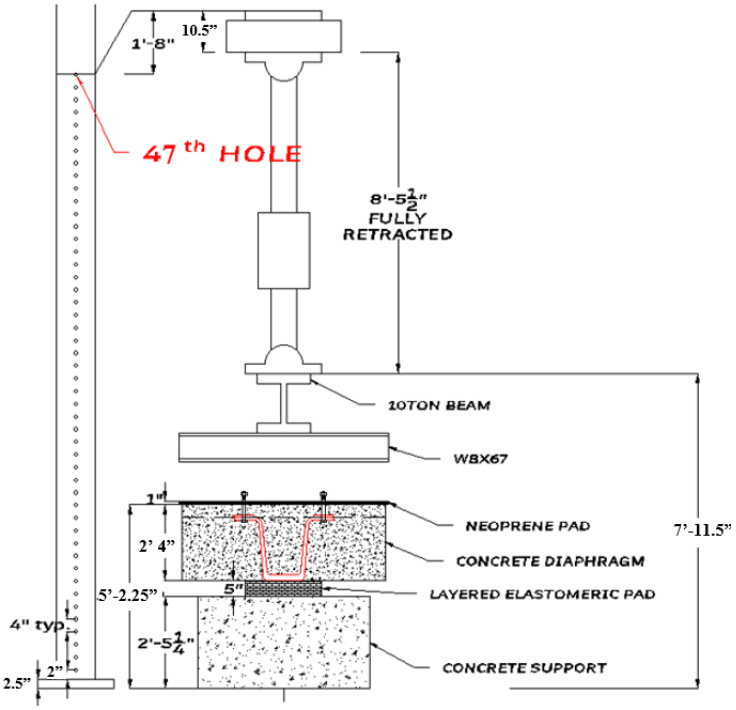


Figure 3-1: Test Set-Up – Rear Elevation

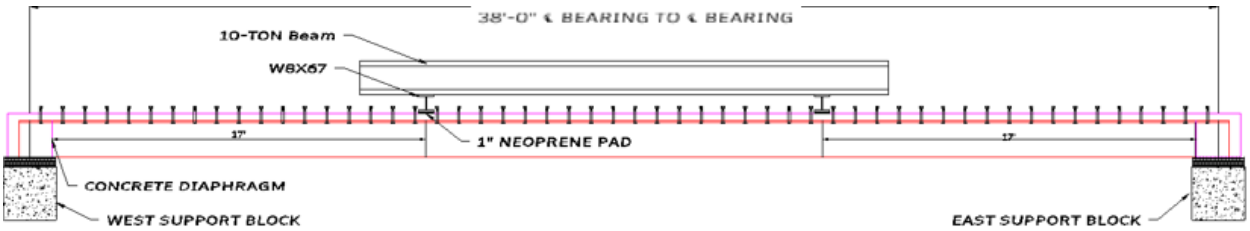


Figure 3-2: Test Set-Up – Side Elevation

UTC-3 was instrumented to measure various aspects of its behavior during testing. Applied load was measured using the load actuator's internal load cell, while displacement at midspan was measured by both the actuator's internal LVDT and a string potentiometer. Support rotations were measured by inclinometers and were also calculated using LVDTs mounted on either side of each support. These LVDTs were also used to measure and correct for the compression of the support bearing pads during loading. Relative slip between the deck and girder was also measured at both ends by LVDTs.

Uniaxial and rosette strain gages were used to measure longitudinal and shear strains, respectively, over the course of strength testing. Uniaxial gages were mounted at the girder's midspan and three feet from midspan to either side with gages mounted on the bottom and top of the bottom flange, on the outside of the webs, on the bottom of the top flange, and on rebar in the deck. These quantified the distribution of strains over the depth of the section, and calculation of the girder's neutral axis. Rosette strain gages were placed on the girder's bottom flange and webs to monitor shear strain at sections 3 feet and 9 feet from the inside face of either support. Finally, stereoscopic cameras were arranged at midspan and girder ends to take successive photos over

the course of testing. These photos could then be used to perform digital image correlation (DIC) to measure the full strain field over the respective parts of the girder.

## 3.3 Results

UTC-3 was successfully tested to failure on February 13, 2023. As planned, it was first subjected to AASHTO Service-I level loading, and then two rounds of AASHTO Strength-I level loading before finally being loaded to failure. Although it was initially planned to load the girder to failure monotonically, incorrectly set limit states within the testing program caused two unintended pauses in loading before eventual failure. This can be seen in Figure 3-3 which presents the total load applied to the girder over the course of the test. Additionally, Figure 3-4 presents the girder's load-deflection response through the entirety of testing with deflection from both the load actuator's internal LVDT and the separate midspan string potentiometer (both corrected for the compression of the neoprene bearing pads under load) which agree well. Figure 3-5 presents the end rotations during testing recorded by inclinometer and calculated by LVDTs at either end of each support. These also tend to agree.

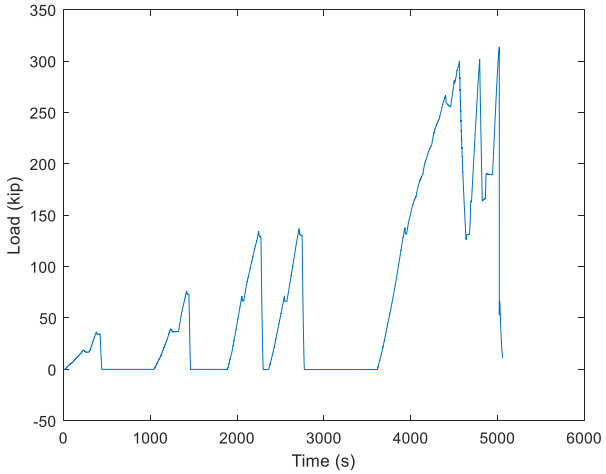


Figure 3-3: Load Applied to UTC-3 over Entire Strength Test

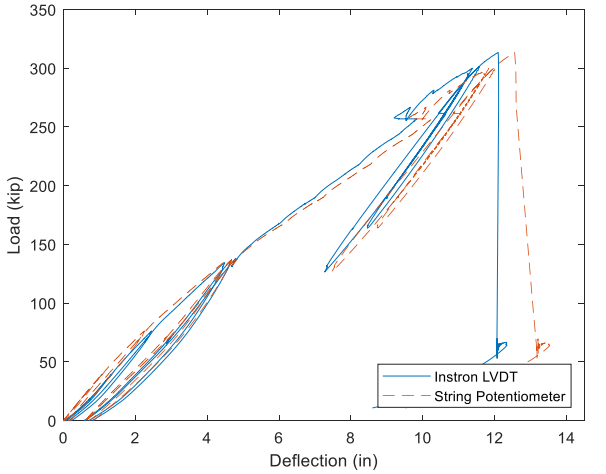


Figure 3-4: UTC-3 Load-Deflection Behavior

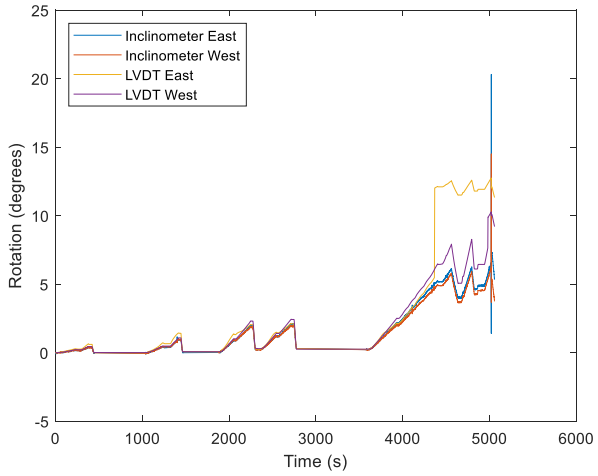

Figure 3-5: Girder End Rotations

As previously mentioned, longitudinal strains were measured at three sections along the span (at midspan and at three feet to either side of midspan) at five vertical locations within the section. This provided thorough insight into the girder's longitudinal bending behavior through the course of testing. Figures 3-6 through 3-8 present the recorded longitudinal strains through the girder depth at three feet east of midspan, midspan, and three feet west of midspan respectively. In general, these strains show that the girder behaved as expected. Strain response tended to increase with increasing load and with an equivalent response at an equivalent load. Additionally, the magnitude of strains tended to change with section depth, indicating a roughly linear strain distribution through the section. It should be noted, however, that at larger loads the larger recorded strains (typically at the bottom flange) began to deviate from expected behavior and so may be less reliable. While the results from bottom flange strain gauges that survived testing are included in the following figures, these strains must be viewed with caution, as they predict strains at failure that we 30 – 40% more than the expected failure strain of about 10,000 $\mu\epsilon$.

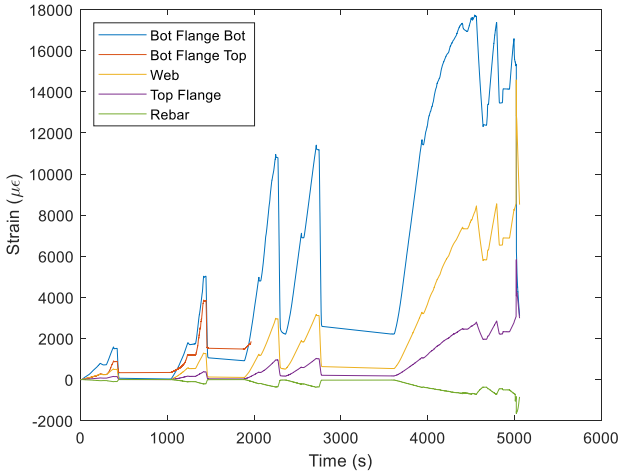

Figure 3-6: Recorded Longitudinal Strains Three Feet East of Midspan

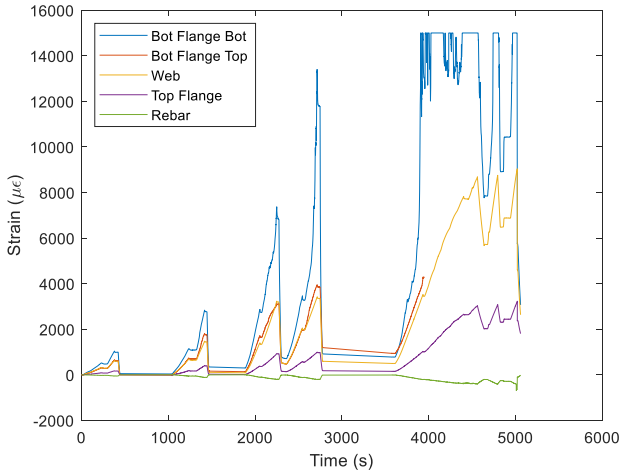


Figure 3-7: Recorded Longitudinal Strains at Midspan

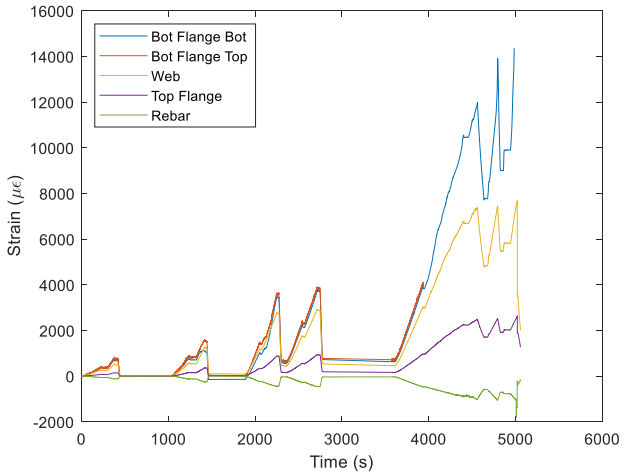


Figure 3-8: Recorded Longitudinal Strains Three Feet West of Midspan

In addition to longitudinal strains, shear strains were recorded during testing at sections three and nine feet from either support. Figures 3-9 through 3-12 show recorded shear strains at three feet and nine feet from the east and west support, respectively. Similar to the longitudinal strains, the shear strains show that the girder behaved generally as expected in shear. As before, strains tended to increase with applied load and were constant for a constant loading level. Shear strains measured at the section bottom tended to be low as expected, except during failure loading. This may indicate malfunctioning of the gages, or higher-than-expected longitudinal strains dominating the response. It is important to note that despite their proximity to the support, the measured shear strains three feet from the supports tended to be smaller in magnitude than those nine feet from the support. This is expected due to the significant reduction in web face sheet thickness between these two sections.

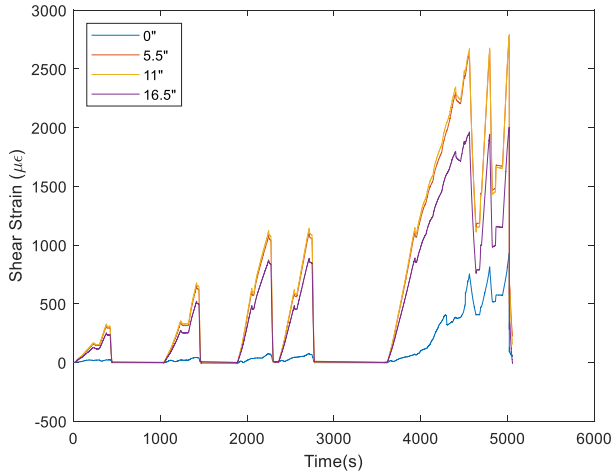


Figure 3-9: Shear Strains Three Feet of East Support

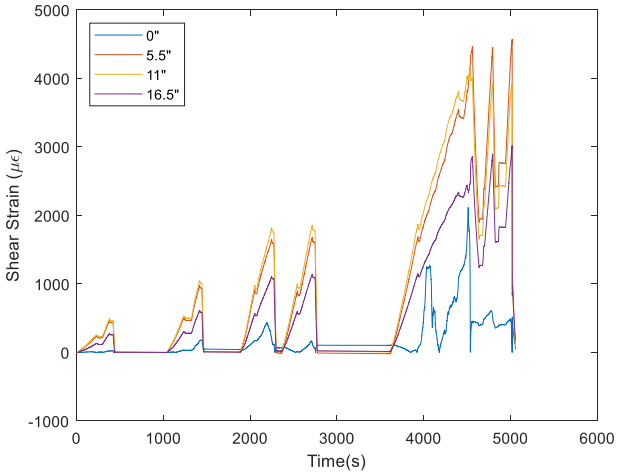


Figure 3-10: Shear Strains Nine Feet of East Support

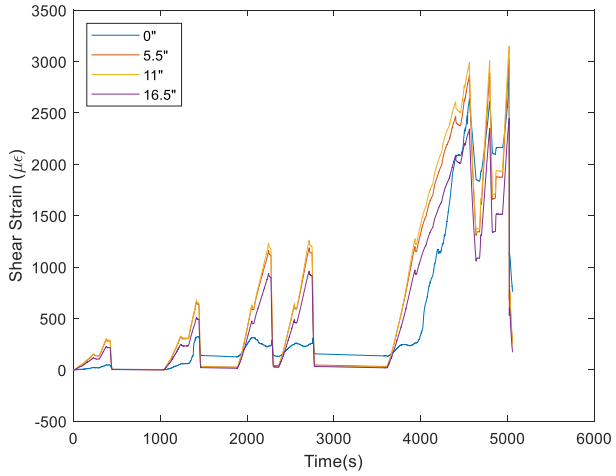


Figure 3-11: Shear Strains Three Feet of West Support

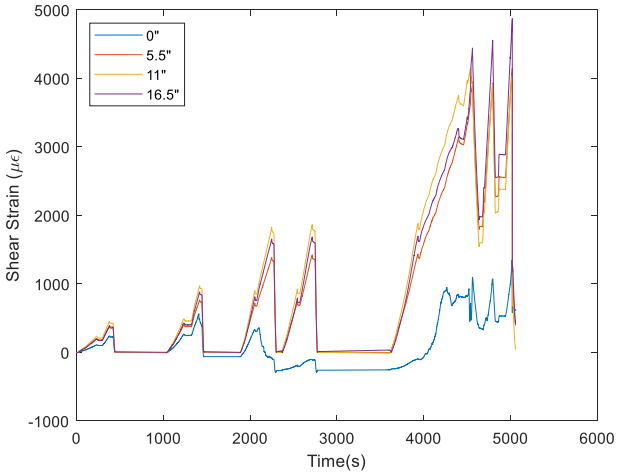


Figure 3-12: Shear Strains Nine Feet of West Support

The girder-deck connection was monitored during testing to evaluate its behavior in a full girder. This involved measuring the relative slip between the girder top flange and deck using LVDTs and evaluating the tension developed in the most heavily loaded shear connectors with a combination of washer load cells and linear strain gages. As seen in Figure 3-13, negligible slip was recorded between the girder and deck during service and strength level loading. During failure loading the slip increased significantly to a maximum of around 0.08 in. Likewise, as seen in Figure 3-14, during the initial loading phases negligible tensile load was measured in the shear connectors. This increased significantly during failure loading, reaching a peak of around 30.0 kip.

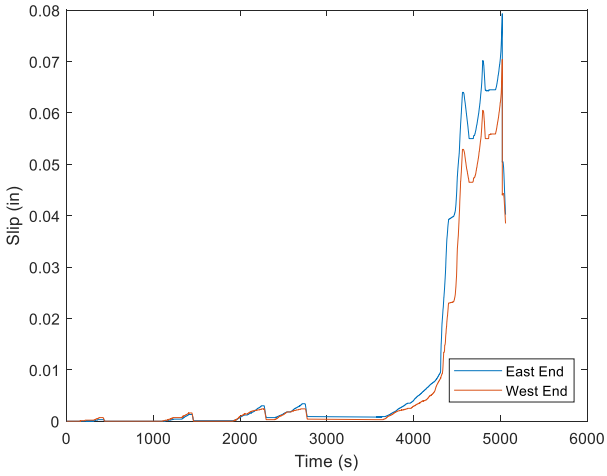

Figure 3-13: Relative Slip

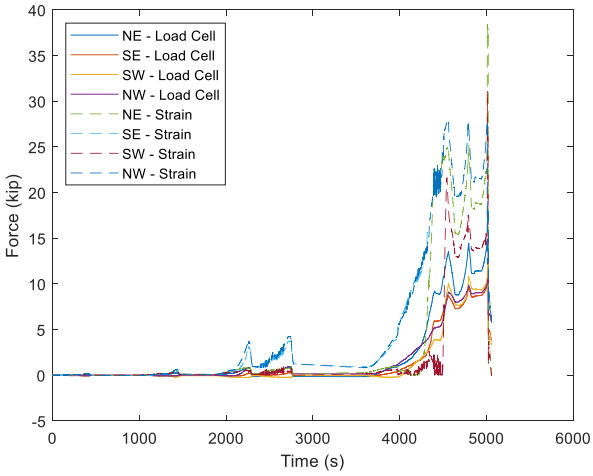

Figure 3-14: Shear Connector Tension

## 3.4 Discussion

The midspan deflection of the girder under Service-I, Strength-I, and maximum loads were predicted and compared with the measured deflection as a way to evaluate the girder's stiffness relative to that which would be used in design. To do this, the girder was modeled as an ideal, simply supported Euler beam under four-point bending and analyzed using the finite difference method. For each node, the moment was first determined by statics. The curvature produced by this moment in the given section was then determined by a nonlinear optimization routine whose objective function was a nonlinear moment-curvature analysis of the girder at the given section. Using the resulting optimized curvatures at all nodes, the finite difference solver could determine the deflection at all nodes – most importantly the maximum deflection at midspan. Shear deformations were then evaluated at the three load levels and added to the Euler deformation predictions to predict deflections as a Timoshenko beam.

Figures 3-15 through 3-18 compare the predicted and measured deflections under Service-I, Strength-I, and at the first and the final ultimate loading levels using both Euler and Timoshenko

beam theories. As can be seen, respectively, predicted deflection under Timoshenko beam assumptions agree reasonably well with measured deflections. This suggests that shear deformations are significant to the overall deformation of the girder under transverse load. As load increases, the predicted deflection decreases relative to the measured deflection. This is seen in Figure 3-19 which compares the maximum measured and predicted deflection with increasing load. It is apparent from Figure 3-19 that the girder behaves in a more compliant manner than is predicted. This could be due, for instance, to irregularities or defects in the composite layup, variability in concrete elastic modulus, or a relatively compliant bottom flange. Figure 3-20 shows the measured and predicted end rotations at failure, which show that very little rotational restraint was experienced.

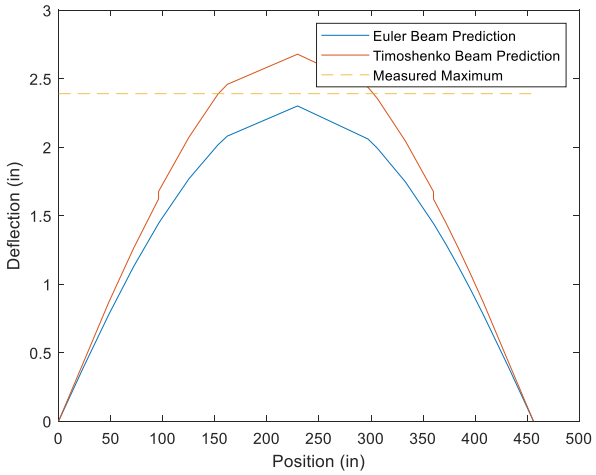


Figure 3-15: Comparison of Predicted and Measured Deflection – Service – I

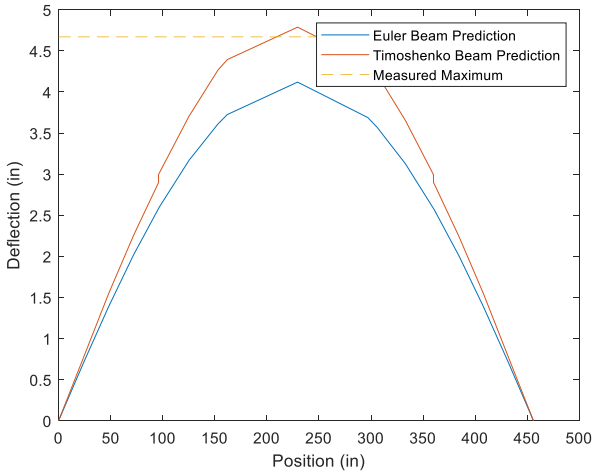


Figure 3-16: Comparison of Predicted and Measured Deflection – Strength - I

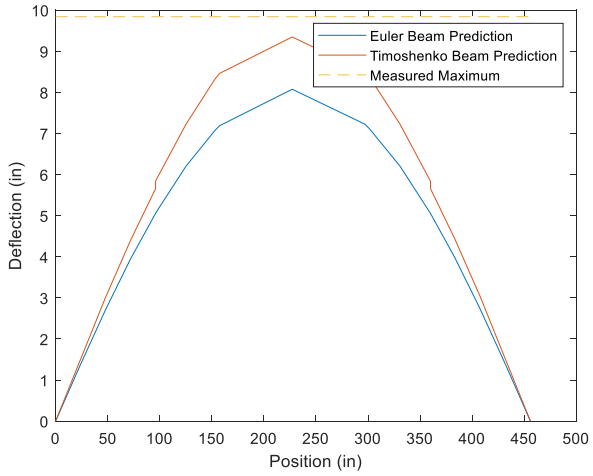


Figure 3-17: Comparison of Predicted and Measured Deflection – First Attempt at Ultimate Load

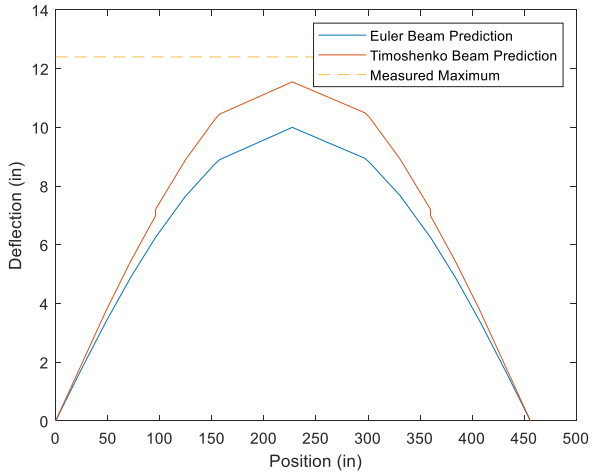


Figure 3-18: Comparison of Predicted and Measured Deflection –Ultimate Load

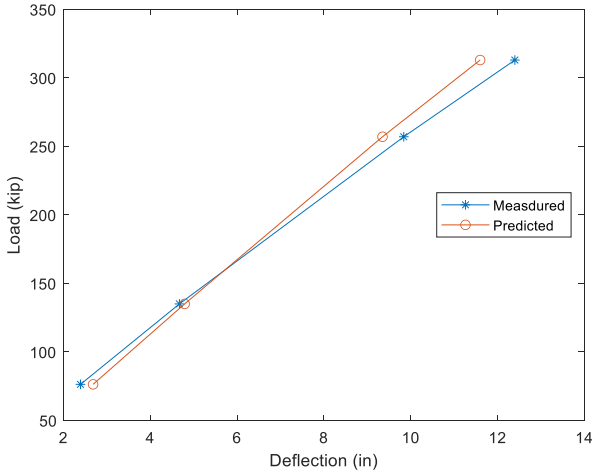


Figure 3-19: Measured and Predicted Mid-span Deflection with Load

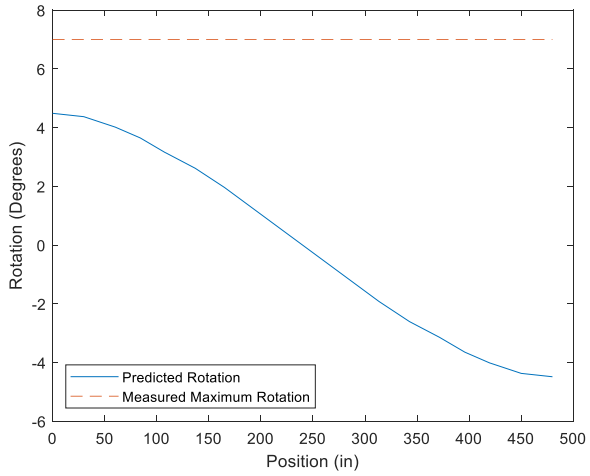

Figure 3-20: Comparison of Predicted and Measured Rotation

Measured longitudinal strains through the girder depth were plotted for the different load levels to examine strain linearity and neutral axis location. This is plotted in Figure 3-21, along with linear fits of the distributions. As can be seen, the distributions are reasonably linear with only small deviations from the best-fit line. This suggests a linear strain distribution as expected. However, as mentioned above, there is doubt of the veracity of strain readings at the bottom of the section for the larger loads, with readings generally larger than expected. This is further evidenced by the maximum strain at the section bottom shown in Figure 3-21, 14.600 με. This must be further increased to account for dead load strain to equal 15,500 με as compared with the expected failure strain of 10,500 με. A review of the literature revealed failure strains for carbon/vinylester composites ranging between 10,300 με and 15,900 με [13-19], putting the measured strains near the upper extreme. It is reasonable to consider a higher rupture strain than the nominal value which is likely the case. However, the unreasonably high strains measured near failure and presented in Figures 3-6 through 3-8 suggest smaller maximum strains.

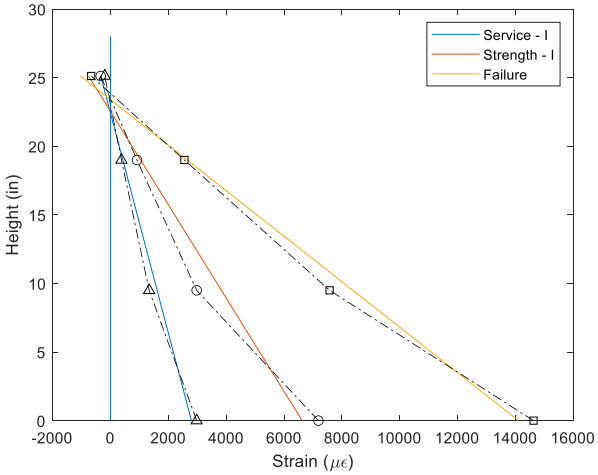

Figure 3-21: Inferred Strain Distributions

To estimate more likely bottom flange strains, the measured bottom flange strains were disregarded, and the strain distributions recalculated. These were then used to extrapolate new

bottom flange strains. This is presented in Figure 3-22. As can be seen, the predicted bottom flange strains become much smaller, with the maximum strain during failure loading being 12,900 με. Adjusting to include dead-load strain gives 13,800 με which, although significantly larger than the nominal value, is closer to the center of the spread of possible failure strains.

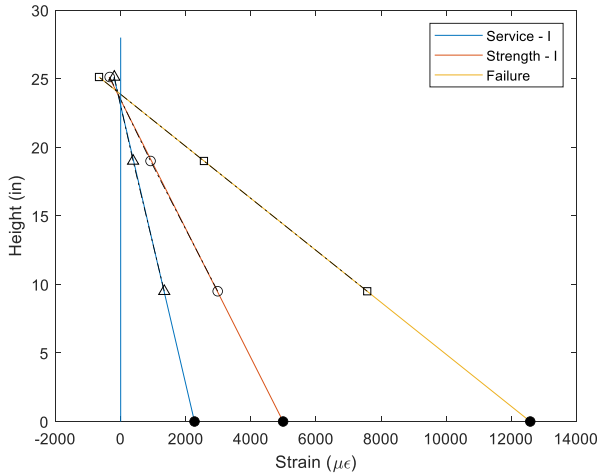


Figure 3-22: Strain Distribution with Extrapolated Bottom Flange Strains

From the strain distribution presented in Figure 3-22, a neutral axis height of approximately 24 in. can be inferred. This is confirmed in Figure 3-23, which presents the calculated neutral axis height based on strains measured throughout testing. Knowing this, the strains measured through the rest of the section can be used to calculate strains at the top of the deck. Doing this yields Figure 3-24, which presents the top-of-deck strains over the course of testing. As can be seen, the maximum concrete strain achieved is around 2,160 με. Being that this is less than the generally assumed concrete crushing strain of 3000 με [12] and considering the high strains inferred in the bottom flange, if is very likely that girder failure came as a result of bottom flange rupture rather than deck crushing.

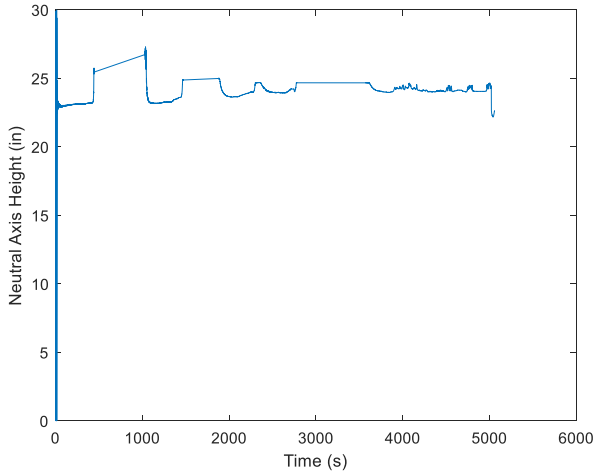


Figure 3-23: Calculated Neutral Axis Height

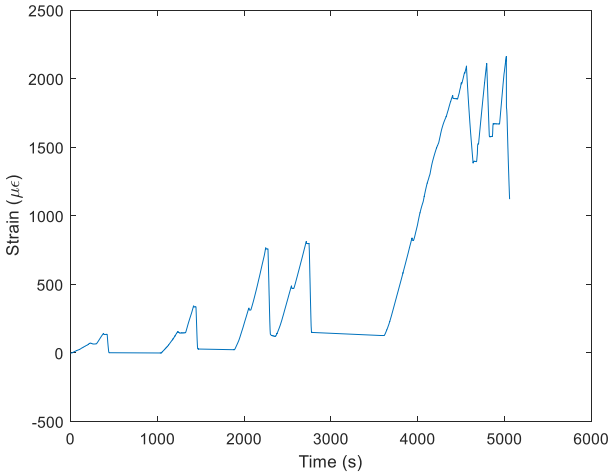

Figure 3-24: Calculated Concrete Strains

Similar to the longitudinal strains, the recorded shear strains through the depth of the section were plotted at the different load levels to compare their distribution with theoretical expectation. This is presented in Figures 3-25 and 3-26 for sections three feet and nine feet from the support, respectively. In these figures the measured strain distributions at Service I, Strength I and failure are plotted along with the predicted theoretical shear strain distribution at failure. As is immediately apparent, the girder's shear response deviated significantly from expectation. Rather than having a parabolic shear strain distribution with a maximum strain at the neutral axis the maximum strains fall consistently around midheight of the web. Additionally, the magnitudes of shear strain at failure are significantly reduced from theory (with the exception of the bottom of the section). The reduced magnitudes of shear strains could result from a higher shear stiffness, which likely is primarily web-driven. However, it is not immediately apparent why the distribution of shear strains differs from that predicted by elementary mechanics principals under the assumption of small shear deformation. As noted above, the girder's midspan deflection was generally more accurately predicted when shear deflections were assumed significant. It is possible that the distribution of shear strains was significantly affected by the shear deflections, leading to the discrepancy seen.

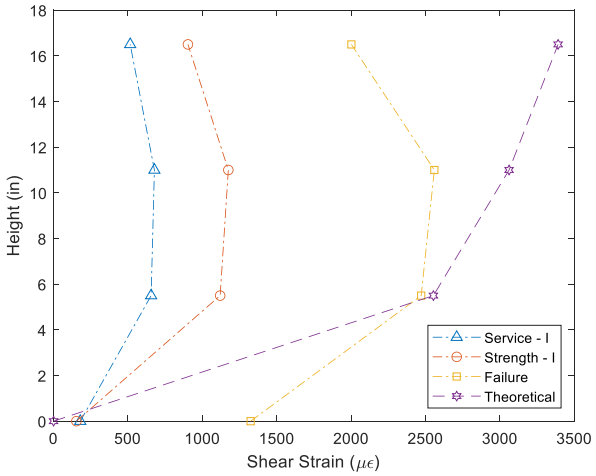

Figure 3-25: Shear Strain Distribution Three Feet from Support

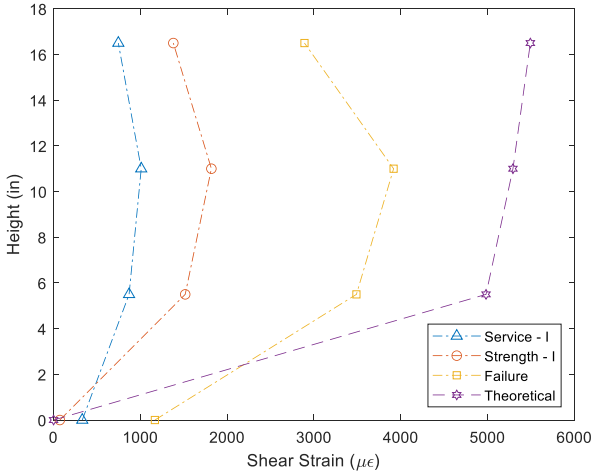

Figure 3-26: Shear Strain Distribution Nine Feet from Support

The results of testing help to further define the behavior of the girder-deck shear connection. At the highest applied load, a shear flow at the girder-deck interface of 5.68 kip/in was generated and withstood by the connection without any visible signs of distress. This is significantly greater than the 4.60 kip/in shear flow maximum previously achieved during push-out testing [8]. One possible reason for this increase in strength is the confining action from the weight of the deck. In the previous push-out tests, specimens were oriented on their sides with only shear connectors providing clamping forces between concrete and FRP. However, when oriented horizontally, the weight of the concrete also aids in keeping the deck and girder in contact, improving the frictional restraint between them and confining the concrete. It is also possible that this improvement by the weight of overlying concrete may have an upper limit of usefulness before which it is less effective. As seen in Figures 3-13 and 3-14, the magnitudes of the slip and bolt tension during the Service I and Strength I ramps are relatively small and with a relatively constant slope. This is also true for the beginning of the failure test. However, at approximately 4,300 s the slope of the slip and bolt tension increase significantly. At this point (under an applied load of around 246 kip) the benefit of the concrete may have been overcome, with all

remaining clamping provided by the shear connectors and thus allowing significant slip and additional bolt tensile forces to develop.

# Chapter 4: Full-Scale CT Girder Fatigue Testing

## 4.1 Introduction

Of the CT girders tested to-date, all but one have been in virgin condition, with one subjected only to self-weight for the purpose of measuring creep and shrinkage deflections. This means that the flexural strengths so far determined have not accounted for loss of stiffness and damage accumulated during a lifetime of service. In addition, most CT girders incorporate a number of fatigue prone details, most notably the inclusion of carbon ply-drops which reduce the number of carbon plies in locations subjected to smaller flexural stresses. For this reason, full-scale CT girder (labeled "UTC-4") constructed with bottom flange ply drops was subjected to repeated load cycling under AASHTO Fatigue – I load to investigate loss of stiffness and potential damage occurrence as a result of repeated loading. It was then statically tested to failure to identify any loss in strength as a result of fatigue loading.

## 4.2 Test Specimen Details and Instrumentation

To simplify comparison of their final flexural strengths, UTC-4 was designed and constructed nominally identically to UTC-2. Following delivery to the ASCC it was fatigue tested over a period of several months, after which failure testing was conducted January 5, 2024. Instrumentation for the failure test of UTC-4 was nominally identical to that of UTC-3. However, fewer strain gages were applied during fatigue testing. This is because strain gages tend not to withstand repetitive loading and testing could not be paused to replace failed gages. Between fatigue and failure testing, most of the accessible gages were replaced as they had either failed or were no longer reliable.

## 4.3 Fatigue Test Protocols

While fatigue life predictions and provisions do not exist for FRP tension flange thickness transitions in bridge girder applications, AASHTO [11] provides clear guidance for assessing the fatigue life of tension flange thickness transitions in steel bridge girders. Since all FRP material was incorporated in the primary girder infusion, the bottom flange ply drop was considered analogous to a continuously welded, partial-length steel cover plate on a steel girder tension flange. AASHTO treats the termination of such a steel cover plate as a Category B fatigue detail, and infinite fatigue life corresponds to the application of 3,000,000 cycles of a factored AASHTO Fatigue I loading with an impact factor of 15%. For the test specimen, the moment produced by the Fatigue I loading at the Zone 2- Zone 3 transition is 460 ft-kip per lane of live loading, and based on the design of the Westerly, RI bridge one girder is responsible for carrying ½ a traffic lane resulting in a 230 ft-kip Fatigue I moment per girder.

Producing this moment at the flange transitions with the 4-point bend configuration of Figure 3-2 requires an applied load of 58.0 kip. To account for additional dead load moment due to a typical 3 in. asphalt wearing surface, the specified load range was 6.0 kip – 64.0 kip, which was applied with a sinusoidal ramp at a rate of slightly less than 0.5 Hz. This was the maximum rate that could be achieved using the available actuator and hydraulic system, and the application of 3,000,000 cycles required approximately 10 weeks of cyclic load testing that was accomplished over a three-month period. The upper bound load of 64.0 kip produced a maximum bottom flange stress at the zone 1 – zone 2 transition of 12.1 ksi, or 11.4% of the ultimate tensile

strength of the bottom flange. Mid-span deflection was recorded with an LDT, as was vertical deflection at each neoprene bearing pad. However, the mid-span several mid-span LTDs failed during testing despite their fatigue rating, and as a result the data from the LDTs recorded during load cycling was not consistent or complete, and actuator position data was therefore used to track specimen displacement. Stiffness tests were run approximately every 100,000 cycles.

## 4.4 Fatigue Test Results

Figure 4-1 shows the mid-span girder displacement range (the difference between measured displacement at the top and bottom of the fatigue load range) with fatigue cycle. The minimum displacement range due to the 58.0 kip fatigue load range was 1.43 in. at the 100$^{th}$ load cycle, and this value increased to 1.91 in. over the course of cycling. As called out Figure 4-1, at about 600,000 cycles the test had to be stopped for several weeks due to a failure of the laboratory fire suppression system, and this was followed by a jump of about 0.080 in. of fatigue cycle displacement. Regardless, for the final 1,500,000 cycles the fatigue range displacement was very stable, ranging between 1.87 in. and 1.91 in. It is important to note that some of the total recorded displacement was likely the result of creep strains and shrinkage of the concrete deck, which were not independently monitored during the test. This is reflected by the change in actuator displacement corresponding to the minimum load of 6.0 kip, which increased by 2.17 in. over the course of the application of 3,000,000 load cycles, with 1.81 in. of this increase occurring during the first 1,500,000 cycles. Further, following completion of fatigue testing, girder mid-span deflection under no load was measured to be 1.57 in.

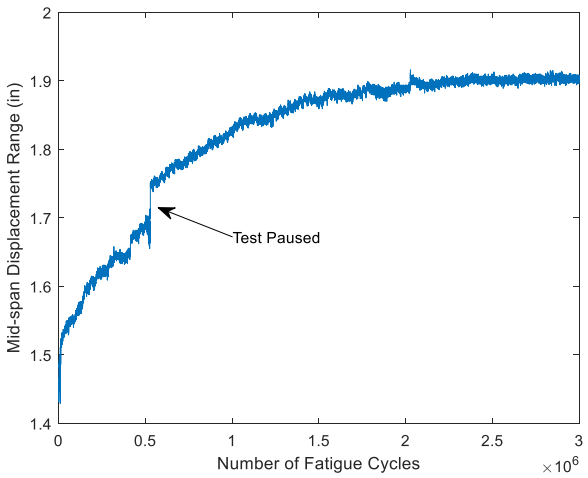


Figure 4-1: Calculated Displacement Range over Fatigue Testing

Stiffness degradation during cycling was tracked by periodically performing pseudo-static load tests up to the maximum Fatigue I load of 64.0 kip. Actuator position was relied upon as the deflection measurement due the aforementioned issues with obtaining independent LDT data during testing. Specimen stiffness was computed for each test as the slope of the best-fit line to the measured load-deflection data over the range of 6.0 kip to 64.0 kip, and stiffnesses are plotted in Figure 4-2. These results show a stiffness loss of 17.5% after the application of 3,000,000 load cycles. Consistent with the results in Figure 4-1, however, the rate of stiffness degradation decreased with increasing fatigue cycles, and most of the stiffness loss occurred in the first 1,500,000 cycles. In line with these quantitative results, no visual signs of damage to the specimen were noted during testing.

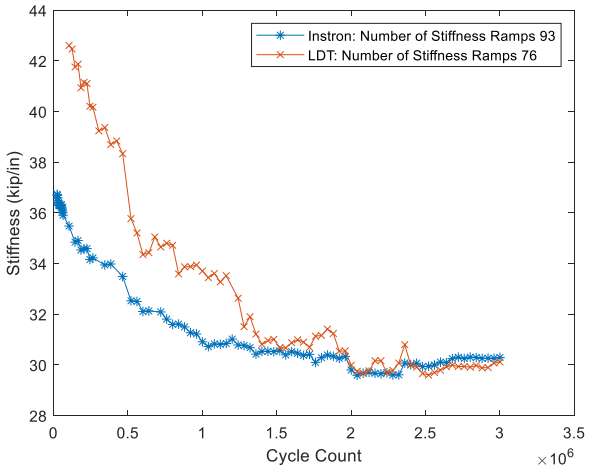

Figure 4-2: Stiffness Degradation over Fatigue Testing

## 4.5 Strength Test Results

UTC-4 was tested to failure on January 5, 2024, using a test protocol identical to that of UTC-3. Figure 4-3 shows load applied as a function of time. As can be seen, UTC-4 experienced catastrophic failure at a load of 212 kip after exhibiting a calculated stiffness of 29.9 kip/in during the load ramp immediately preceding the final ramp to failure. This is in contrast to the 313 kip load achieved by UTC-3 at a stiffness of 33.9 kip/in, drops of 32.3% and 11.8%, respectively. Figure 4-4 shows the load-displacement behavior of the girder over the course of testing, using displacements measured by both the external, midspan LDT and the actuator's internal LVDT, both corrected to account for compression of the elastomeric bearing pads. Deflections measured by both methods tend to agree well. Slip between the deck and girder were also measured with separate LVDTs, the data from which are presented in Figure 4-5. As can be seen, the measured slips were insignificant, indicating full composite action at all levels of load.

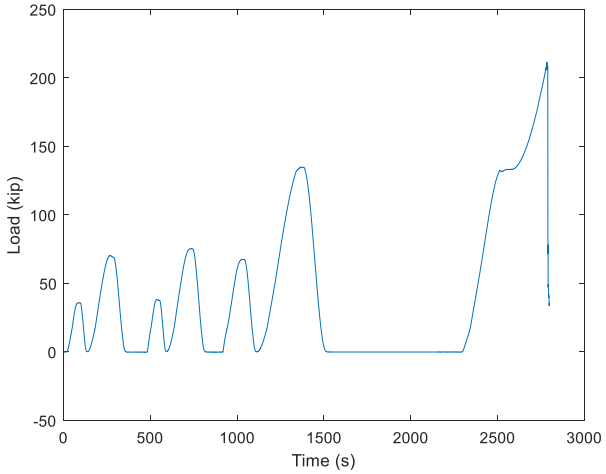

Figure 4-3: Strength Test Loading Sequence

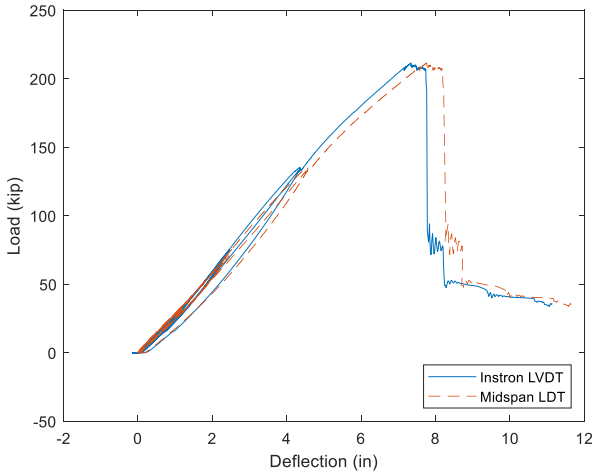

Figure 4-4: Load Displacement during Strength Testing

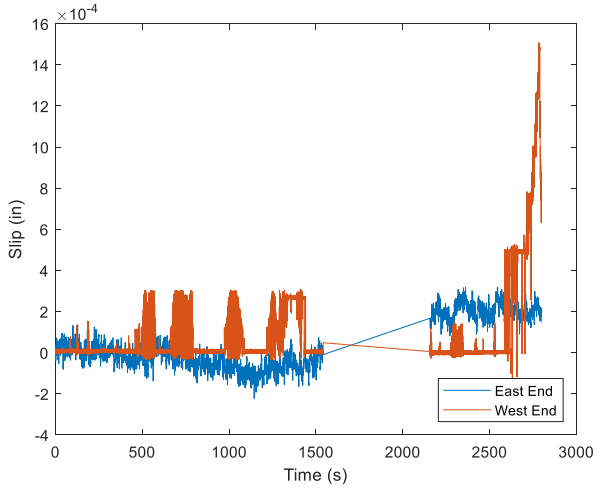

Figure 4-5: Measured Slip Between Girder and Deck

As with UTC-3, longitudinal and shear strains were recorded continuously over the course of strength testing UTC-4. Unfortunately, however, due to malfunctions in the data acquisition hardware, significant portions of the strain data were corrupted including all bottom flange longitudinal strains and some shear strains near the neutral axis. This limits the ability to infer behavior definitively, but the data still reveal useful information. Figures 4-6 through 4-8 show longitudinal strains measured three feet east of midspan, at midspan, and three feet west of midspan, respectively, over the course of testing. These show strains that increase with distance from the neutral axis as expected, and a relative uniformity of strains in the constant moment region from which they were measured. These also show increases in strain proportional to increase in load, as expected.

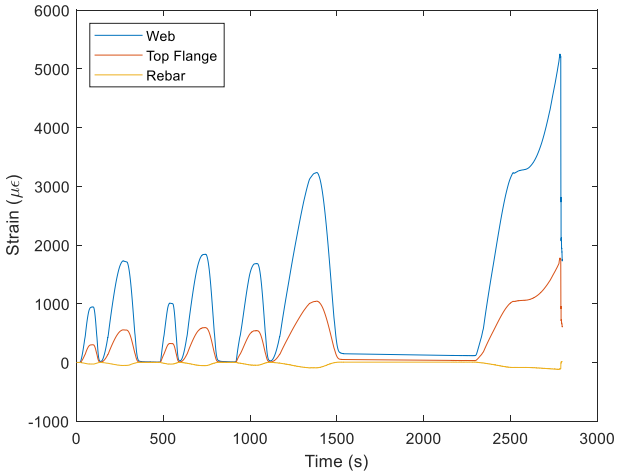


Figure 4-6: Longitudinal Strains Measured 3 feet East of Midspan

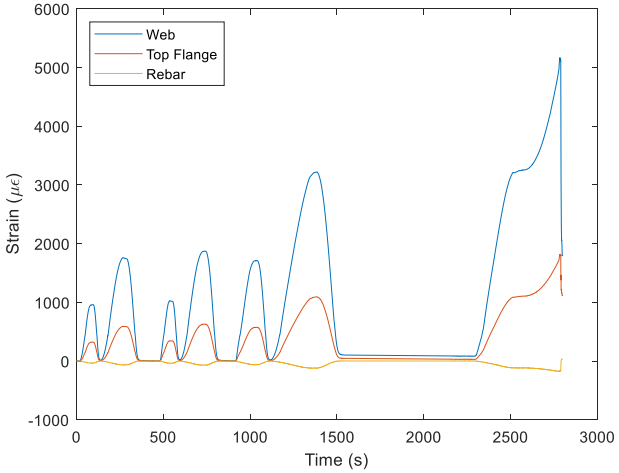


Figure 4-7: Longitudinal Strains Measured at Midspan

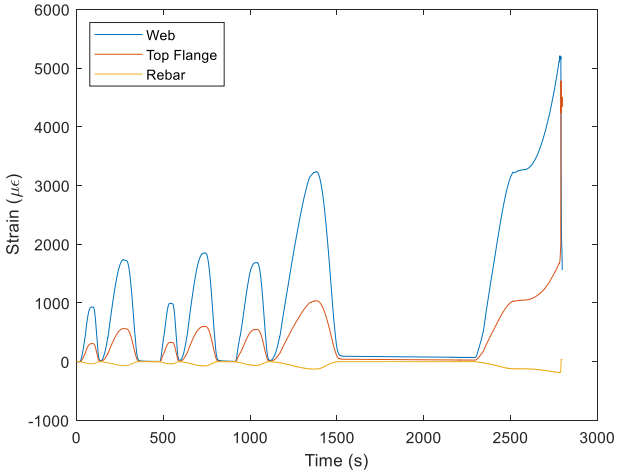


Figure 4-8: Longitudinal Strains Measured 3 feet West of Midspan

Figures 4-9 through 4-12 present shear strains measured over the course of strength testing at sections 3 feet and 9 feet from the east bearing and at sections 9 feet and 3 feet from the west bearing, respectively. As in the test of UTC-3, shear strains tended to increase proportionally to load and returned to zero upon unloading (except at failure). Generally, shear strains nearer to the bottom of the section tended to be smaller in magnitude than those higher up in the section as expected. This is true at all sections except the section 3 feet from the west support. In this case the measured strains seem to indicate the opposite effect. This may be due to a mislabeling of channels in the data acquisition hardware or a malfunction in one or more of the legs of the 5.5-inch-high strain rosette. As in the test of UTC-4, the shear strains measured further from the support tended to be larger in magnitude due to the difference in web facesheet thickness in the two locations.

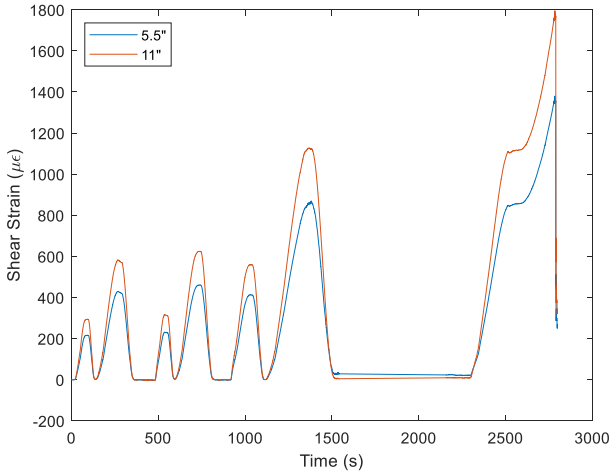


Figure 4-9: Shear Strains Measured 3 feet from the East Support

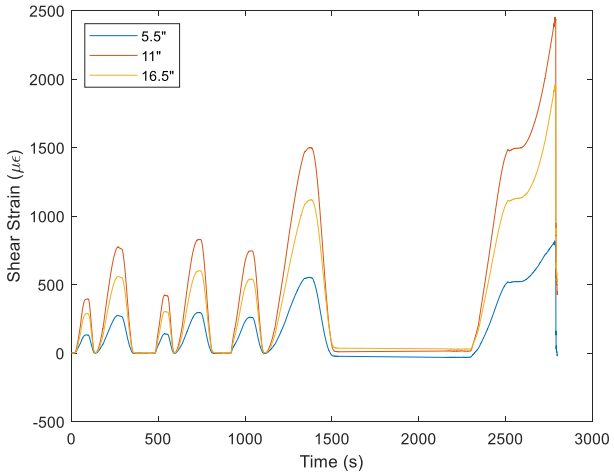


Figure 4-10: Shear Strains Measured 9 feet from the East Support

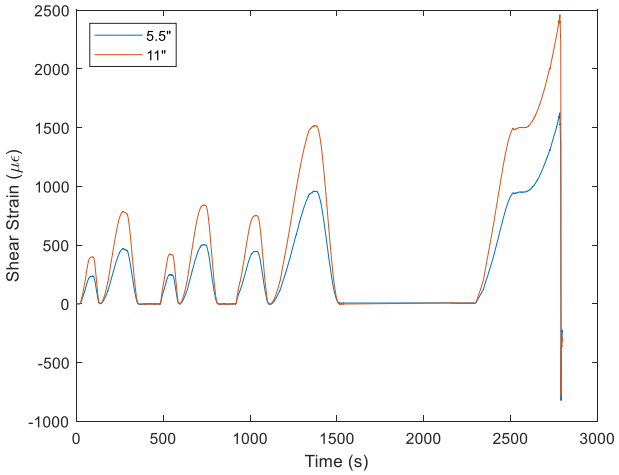


Figure 4-11: Shear Strains Measured 9 feet from the West Support

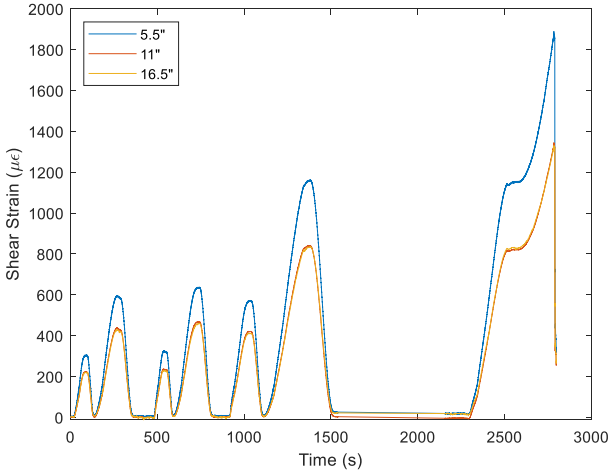


Figure 4-12: Shear Strains Measured 3 feet from the West Support

## 4.6 Discussion

As mentioned above, UTC-4 failed at a significantly lower load than UTC-3 (32.3% lower) and had a significantly lower stiffness (11.8%) during strength testing. Although creep and shrinkage effects should not be completely discounted, it is likely that the effects of fatigue loading accounts for much of this difference. During the fatigue test, significant load was applied repeatedly which was designed to maximize stress at the location of the ply-drop. However, in maximizing this stress, additional stresses were encountered at midspan. This could have combined to produce an overload which allowed more significant damage to accumulate. In addition, as seen in Figure 4-13, failure occurred directly beneath the load-head and caused fracture in both the bottom flange and webs. This combines to suggest that failure may have been due to combined flexural and shear stresses in the vicinity of loading.

Figure 4-13: Image UTC-4 of Failure Location and Damage

Like with UTC-3, the deflection of UTC-4 was predicted under Fatigue-I, Service-I, Strength-I, and ultimate loading levels. These predictions were made by solving the boundary value problem with a finite difference solution technique under Euler-Bernoulli and Timoshenko beam theory assumptions. The results of these analyses are compared with measured deflection at corresponding load levels in Figures 4-14 through 4-17. As can be seen, the analyses that used Euler-Bernoulli assumptions tended to consistently underpredict midspan deflection, whereas Timoshenko assumptions overpredicted deflections by a smaller amount. This suggests that, like UTC-3, shear deflections are significant and should be considered.

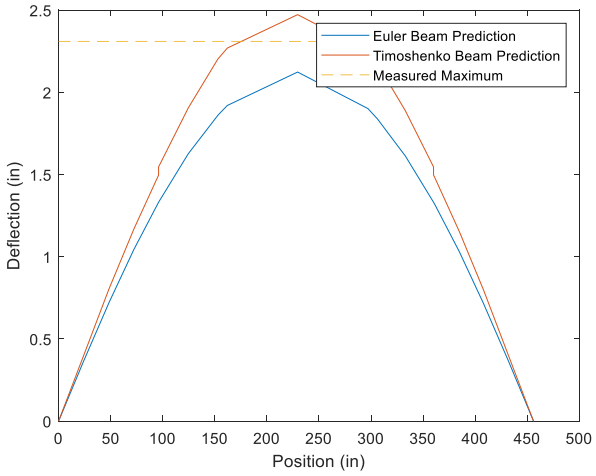


Figure 4-14: Comparison of Predicted and Measured Deflections under Fatigue-I Loading

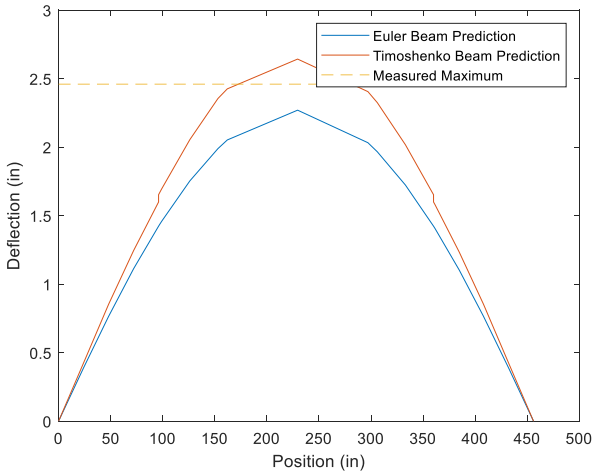


Figure 4-15: Comparison of Predicted and Measured Deflections under Service-I Loading

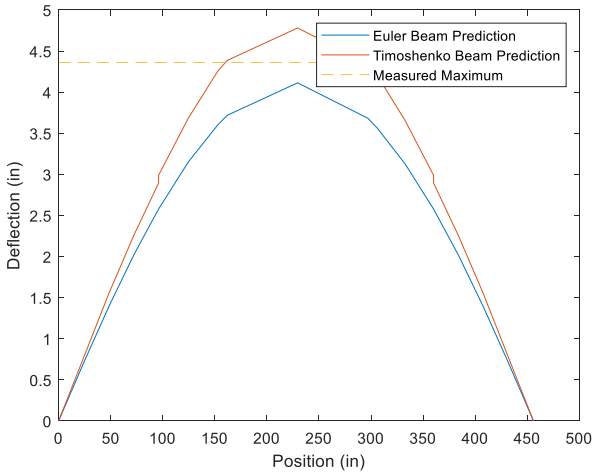


Figure 4-16: Comparison of Predicted and Measured Deflections under Strength-I Loading

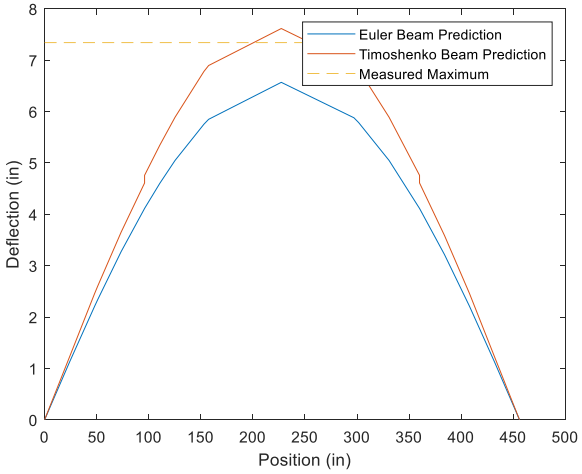


Figure 4-17: Comparison of Predicted and Measured Deflections under Failure Loading

Measured longitudinal strains were plotted with height to determine the location of the neutral axis within the section. This can be seen in Figure 4-18 along with lines of best fit through these points. As can be seen, the neutral axis fell at approximately 24.3 inches from the bottom of the section at all levels of loading. This compares well with the neutral axes found when testing UTC-3. From the line of best fit for strains measured at a failure load of 212 kip, the strain at the bottom flange at midspan was projected to reach a magnitude of about 7750με. This compares well with the projected strain at 313 kip from UTC-3 as shown in Figure 3-22, showing a linear increase from one to the other. These observations combine to suggest that fatigue cycling did not significantly impact the elastic behavior of the girder.

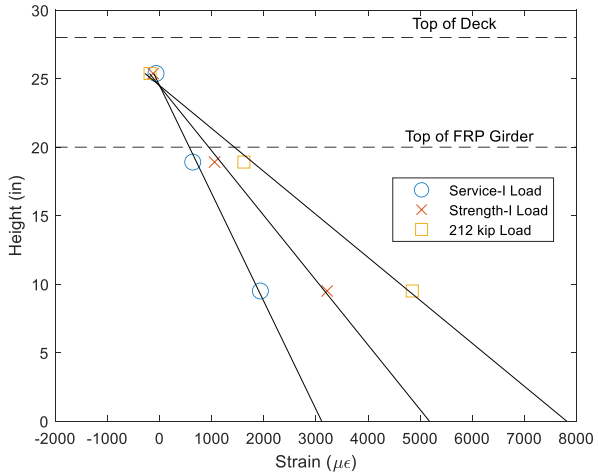


Figure 4-18: UTC-4 Longitudinal Strain Distribution

As with longitudinal strains, shear strains were also plotted with height as seen in Figures 4-19 and 4-20 averaged for the sections 3 feet and 9 feet from the supports, respectively. The shapes of these distributions are similar to those of UTC-3, which is in contrast to the theoretically parabolic distribution expected. This is consistent with both girders' significant shear deflection as discussed above and provides further evidence of their similarity in elastic behavior.

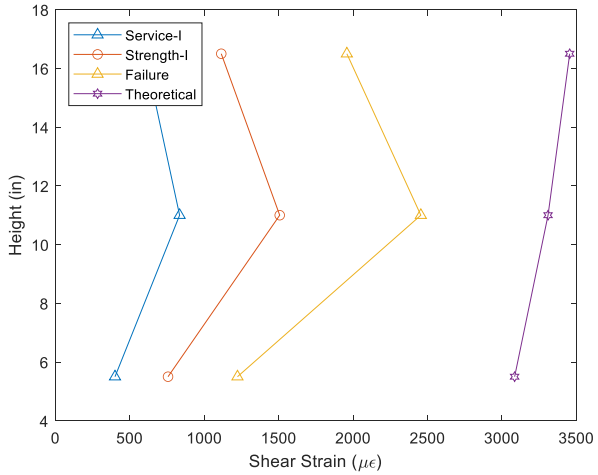


Figure 4-19: Shear Strain Distribution 3 feet from Support

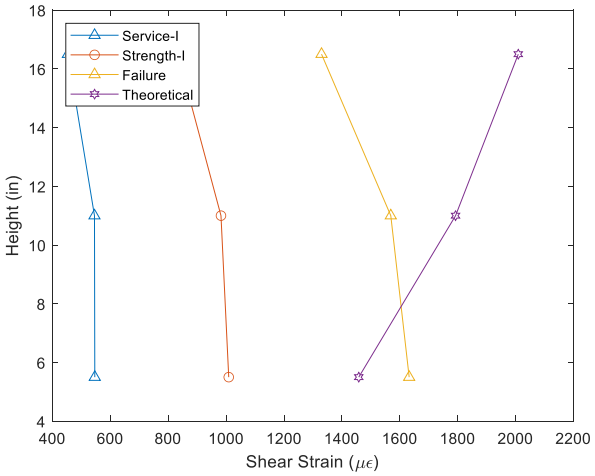

Figure 4-20: Shear Strain Distribution 9 feet from Support

# Chapter 5: Conclusions and Recommendations

The results of shear block testing indicate that the FRP connectors used in this study do not provide consistently adequate stiffness, strength and fatigue resistance required for implementation. The residual strength of the two specimens successfully tested to 6,000,000 fatigue cycles was 30%-35% less than that of similar specimens fabricated with the stainless steel connectors currently used in practice, and their stiffness was much lower relative to current connectors.

The strength test of the full-scale girder gave consistently good results that were in line with expectations. The observed girder strength and stiffness were close to predicted values, and the shear connectors performed well. This test further confirms both the adequacy of the GBeam and the appropriateness of current design methodologies, including that used for the shear connectors where connector tension is assumed to mobilize the shear friction connection between the girder and deck.

The girder fatigue test was also successful in that the specimen sustained 3,000,000 cycles of factored fatigue load and retained approximately 67% of its original strength post-fatigue. To put this in perspective, the girder had a flexural capacity after fatigue of approximately 1.4 times the factored AASHTO Strength I moment based on the original design parameters. Further, the failure did not occur at the bottom flange ply drop, which indicates that properly detailed and fabricated ply drops may not be a problem for fatigue.

Future research should focus on two areas to further advance and fully understand GBeam behavior as detailed below.

- *The development of improved FRP shear connectors that provide sufficient strength and stiffness.* A weak link in the system tested here was the FRP nuts installed on the FRP bars, and the development of a connector that relies on a mechanical wedge to mobilize its tensile capacity might be beneficial. Shear connector tension forces measured during the girder strength test and their coincidence with increasing girder-deck slip reinforce the importance of using an FRP shear connector that can develop substantial tension to mobilize the shear-friction interface. Further, tighter connector spacing might be required when FRP shear connectors are used in lieu of stainless steel.

- *Further analysis of fatigue test results.* While the significant residual strength of the fatigued specimen is a positive test outcome, a more rigorous analysis of the fatigue test results to quantify girder fatigue life under realistic truck loading spectra would be very beneficial. Ultimately, a quantitative fatigue damage model should be implemented. Such a model will allow the rational development of practical fatigue design guidelines such as an explicit limit on fatigue load-induced tensile stress in the bottom flange.

## References


[1] Guzzi, D. (2017). Milestone 25: Conceptual Design of Joints. University of Maine, Orono.

[2] Guzzi, D. (2019). Shear Connectors for Hybrid Composite FRP-Concrete Bridge Girders. University of Maine, Orono.

[3] Guzzi, D. (2017). Milestone 26: Detailed Joint Design. University of Maine, Orono.

[4] Guzzi, D. (2017). Milestone 27: Preliminary Laboratory Joint Testing. University of Maine, Orono.

[5] Guzzi, D. (2018). Milestone 28: Detailed Joint Testing of Downselected Designs. University of Maine, Orono.

[6] Guzzi, D. (2019). Milestone 29: Final Joint Testing. University of Maine, Orono.

[7] Schanck, A. (2020). Milestone 25: Develop Additional Joints Concepts, Manufacture Scale Test Articles, and Perform Static and Fatigue Tests. University of Maine, Orono.

[8] Schanck, A., Diba, A., and Davids, W. (2022). Assessment and optimization of double CT bridge girder sections with longitudinal precast decks. University of Maine, Orono.

[9] Davids, W., Diba, A., Dagher, H., Guzzi, D., and Schanck, A. (2022). Development, assessment, and implementation of a novel FRP composite girder bridge. *Construction and Building Materials*. 340(2022).

[10] Davids, W., Guzzi, D., and Schanck, A. (2022). Development and experimental assessment of friction-type shear connectors for FRP bridge girders with composite concrete decks. *Materials.* 15(9): 3014-3034.

[11] AASHTO. (2012). AASHTO LRFD Bridge Design Specifications, Washington, D.C.: AASHTO.

[12] ASTM International. (2020). C39/C39M-20 Standard Test Method for Compressive Strength of Cylindrical Concrete Specimens. West Conshohocken, PA: ASTM International.

[13] Broyles N. S., Verghese, K. N. E., Davis, R. M., Lesko, J. J., & Riffle, J. S. (2005). Pultruded carbon fiber/vinyl ester composites processed with different fiber sizing agents. Part I: Processing ad static mechanical performance. *Journal of Materials in Civil Engineering.* 17(3): 320-333.

[14] Pirvu, A., Gardner, D. J., & Lopez-Anido, R. (2004). Carbon fiber-vinyl ester composite reinforcement of wood using the VARTM/SCRIMP fabrication process. *Composites: Part A.* 35(2004): 1257-1265.

[15] Marouani, S., Curtil, L., & Hamelin, P. (2012). Ageing of carbon/epoxy and carbon/vinylester composites used in the reinforcement and/or the repair of civil engineering structures. *Composites: Part B*. 43(2012): 2020-2030.

[16] Tan, T. T. M., & Nieu, N.H. (1996). Hybrid carbon-glass fiber vinyl ester resin composites. *Die Angewandte Makromolekulare Chemie.* 234(1996): 53-58.

[17] Suresha, B., & Kumar, K. N. S. (2009). Investigations on mechanical and two-body abrasive wear behavior of glass/carbon fabric reinforced vinyl ester composites. *Materials and Design*. 30(2009) 2056-2060.

[18] Figiolini, A.M. (2011). Degradation of Mechanical Properties of Vinylester and Carbon Fiber/Vinylester Composites Due to Environmental Exposure. Master's Thesis: Florida Atlantic University, Boca Raton, FL.

[19] José-Trujillo, E., Rubio-González, C., & Rodríguez-González J.A. (2019). Seawater ageing effect on the mechanical properties of composites with different fiber and matrix types. *Journal of Composite Materials*. 53(23):3229-3241.

# Appendix A: Additional Tables and Figures

The quality of the ridges in the shear-plates used during this generation of shear block testing is shown below in Table **Error! No text of specified style in document.**-1 below. Imperfections were considered any divots in the ridges equal to greater than 0.25 in. in width and depth. The more shaded a cell is the worse that ridge's quality was.

**Table** Error! No text of specified style in document.**-1: Shear-Plate Ridge Quality**

| | Total Imperfection Width (top to bottom, in) | | | | | | | | | |
|---|---|---|---|---|---|---|---|---|---|---|
| Ridge No. | 1A | 1B | 2A | 2B | 3A | 3B | 4A | 4B | 5A | 5B |
| 1 | 0.75 | 0 | 0 | 0 | 4.5 | 0.25 | 0 | 0.5 | 0 | 4.5 |
| 2 | 3 | 0 | 0 | 0 | 2 | 0.5 | 0 | 0.25 | 0.75 | 5.5 |
| 3 | 3.5 | 0 | 2.5 | 0 | 3 | 0 | 0 | 0 | 0.5 | 4.25 |
| 4 | 4.5 | 4.5 | 3 | 0 | 3.25 | 0 | 0 | 0 | 0 | 2.5 |
| 5 | 6 | 3.5 | 0 | 0 | 1.5 | 0 | 0 | 0 | 0 | 1.25 |
| 6 | 3 | 3 | 5 | 0 | 3.25 | 0 | 0 | 0 | 0 | 1.5 |
| 7 | 3.5 | 4 | 1 | 0 | 0 | 0 | 0 | 0.5 | 0 | 2.5 |
| 8 | 4.75 | 3 | 0 | 0 | 3 | 0 | 0 | 0 | 0 | 4.25 |
| 9 | 0 | 2.5 | 1.235 | 0 | 5.5 | 0 | 0 | 0 | 0.25 | 0.25 |
| 10 | 0 | 1.5 | 5 | 0 | 4 | 0 | 0 | 0 | 0.5 | 0 |
| 11 | 0 | 4.25 | 1.5 | 0 | 0.75 | 0 | 0 | 0 | 0.5 | 1.5 |
| 12 | 0 | 5.5 | 5 | 0 | 2 | 0 | 0 | 0.75 | 0.5 | 0 |
| 13 | 2.5 | 5.75 | 2.25 | 0 | 4.75 | 0 | 0 | 0.75 | 5.25 | 1.75 |
| 14 | 0.25 | 5 | 1 | 0 | 3 | 0 | 0 | 0.25 | 0.25 | 0.5 |
| 15 | 3 | 5.25 | 1.25 | 0 | 2.5 | 0 | 0 | 0.5 | 5 | 2.5 |
| 16 | 2.5 | 4.5 | 0.75 | 0 | 4.5 | 0 | 0 | 0.25 | 0.75 | 0 |
| 17 | 1 | 2.5 | 0 | 0 | 4.75 | 0 | 0 | 0.25 | 2 | 0 |
| 18 | 2.25 | 3.25 | 0 | 0 | 2.5 | 0 | 0 | 0.5 | 0 | 0 |
| 19 | 2.5 | 2.5 | 0 | 0 | 3.75 | 0 | 0 | 0.5 | 0 | 1.75 |
| 20 | 4.5 | 6 | 0 | 0 | 2 | 0 | 0 | 0.25 | 0 | 0 |
| 21 | 4.75 | 5.25 | 5 | 0 | 0.75 | 0 | 0 | 0 | 0 | 0.5 |
| 22 | 3.5 | 6 | 0 | 0 | 2.5 | 0 | 0 | 0.25 | 0.5 | 0.75 |
| 23 | 1.75 | 2.25 | 0.5 | 0.25 | 2 | 0 | 0 | 0.25 | 0.25 | 0 |
| 24 | 2.75 | 4.5 | 0 | 0 | 0.5 | 0 | 0 | 0.25 | 0 | 0 |
| 25 | 0.75 | 3.5 | 0 | 0 | 2.5 | 0 | 0 | 0 | 0 | 0 |
| 26 | 0 | 4 | 0 | 0 | 1.25 | 0 | 0 | 0.75 | 0 | 0 |
| 27 | 1 | 2.25 | 0 | 0 | 2.75 | 0 | 0 | 0.5 | 0 | 0 |
| 28 | 2.5 | 4.25 | 0 | 0 | na | 0 | 0 | na | 0 | 0.25 |
| total length | 64.5 | 98.5 | 34.985 | 0.25 | 72.75 | 0.75 | 0 | 7.25 | 17 | 36 |
| % Imper. | 38% | 59% | 21% | 0% | 43% | 0% | 0% | 4% | 10% | 21% |

Shown in Table **Error! No text of specified style in document.**-2 are the concrete cylinder compressive strength testing that was conducted periodically throughout testing. Testing was in accordance with ASTM C39 Standard Test Method for Compressive Strength of Cylindrical Concrete Specimens for 4x8 in. specimens. Testing was spread out since there was not enough specimens to test at every milestone.

**Table** Error! No text of specified style in document.**-2: Concrete Compressive Strength**

| *Date* | *Compressive Strength (ksi)* | *Corresponding Shear Block* |
|---|---|---|
| 1.14.2022 | 6.20 | 3 |
| 1.14.2022 | 7.20 | 3 |
| 1.14.2022 | 7.61 | 3 |
| 2.8.2022 | 8.23 | 2 |
| 2.8.2022 | 8.94 | 2 |
| 2.8.2022 | 8.80 | 2 |
| 4.6.2022 | 8.52 | 5 |
| 4.6.2022 | 8.96 | 5 |
| 4.6.2022 | 8.68 | 5 |
| 8.1.2022 | 9.73 | 4 *(Failure)* |
| 8.1.2022 | 10.0 | 4 *(Failure)* |
| 8.3.2022 | 9.56 | 2 *(Failure)* |
| 8.3.2022 | 9.59 | 2 *(Failure)* |

Figure **Error! No text of specified style in document.**-1 and Figure **Error! No text of specified style in document.**-2 are the average accumulated slips of shear blocks 2 and 3 as a function of load at the load cycles shown in each of their keys. The horizontal distance between the curves is the average slip accumulated between the two cycles. The clockwise rotation from the curves left to right is the decreasing stiffness of the load cycle, meaning there is more intracycle slip later in testing. Lastly, a difference in loading and unloading cycles would indicate hysteresis from the loading, and likely the accumulation of damage.

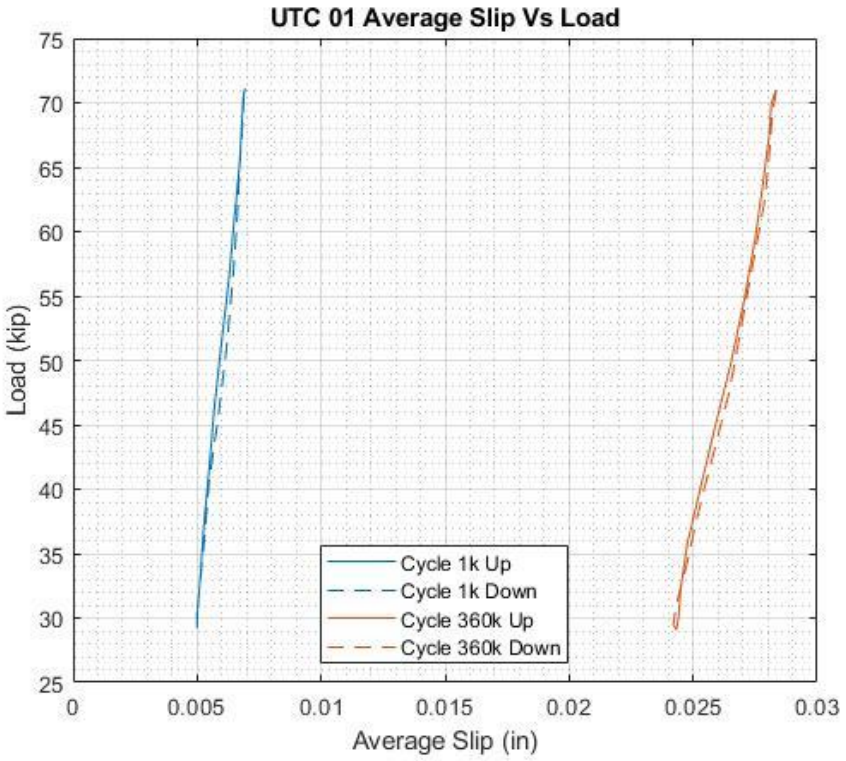


**Figure** Error! No text of specified style in document.**-1: Shear Block 1 Average Slip Vs Load**

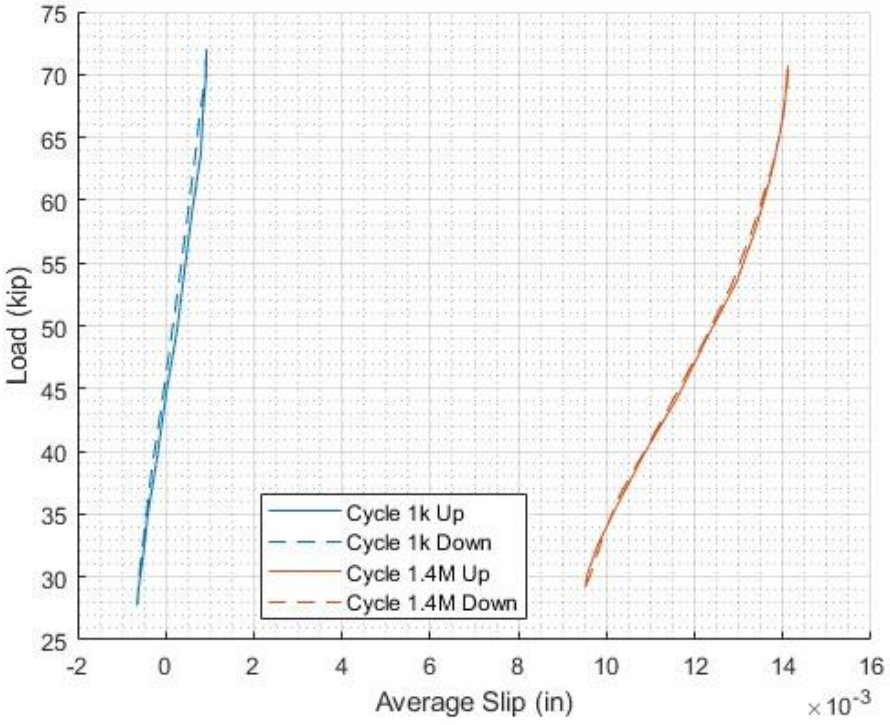


**Figure** Error! No text of specified style in document.**-2: Shear Block 3 Average Slip Vs Load**

# Appendix B: Shear Flow and Fatigue Loading Calculations

## Double CT Girder Fatigue- Loading Calculations

Bridge Details

$L := 53\ ft$ — Span Length

$t_{ws} := 0\ in$ — Wearing Surface Thickness

$n_{stud} := 2$ — Number of Studs per Row

$I_{transPre} := (8.44210 \cdot 10^3)\ in^4$ — Precomposite Transformed Moment of Inertia

$Q_{Pre} := 418.18\ in^3$ — Precomposite Transformed 1st Moment of Area to Shear Plane

$I_{transPost} := (1.7546 \cdot 10^4)\ in^4$ — Postcomposite Transformed Moment of Inertia

$Q_{Post} := 697.88\ in^3$ — Postcomposite Transformed 1st Moment of Area to Shear Plane

Dead Loading

$V_{Pre} := 24.53\ kip$ — Precomposite Dead Load Shear

$V_{Barrier} := 2.36\ kip$ — Shear from Barriers (Estimated)

$V_{ws} := 0\ kip$ — Wearing Surface Shear (Composite Wearing Surface)

## Strength I Shear Loading

$\gamma_{LL} := 1.75$ $\quad IM := 1.33$ — Load and Impact Factors

$\gamma_{DW} := 1.5$ $\quad \gamma_{DC} := 1.25$

$g_v := 0.5$ — Shear Distribution Factor

$P_{front} := 8\ kip$ — Axle Loads

$P_{back} := 32\ kip$

$s := 14\ ft$ — Axle Spacing

$w_{lane} := 0.64\ \frac{kip}{ft}$ — Lane Load

$V_{truck} := P_{back} \cdot \left(1 + \frac{L-s}{L}\right) + P_{front} \cdot \left(\frac{L-2 \cdot s}{L}\right) = 59.321\ kip$ — Shear from Load Tuck

$V_{lane} := \frac{w_{lane} \cdot L}{2} = 16.96\ kip$ — Shear from Lane Load

$V_{LL} := g_v \cdot (V_{truck} \cdot IM + V_{lane}) = 47.928\ kip$ — Live Load Shear

$V_u := \gamma_{DW} \cdot V_{ws} + \gamma_{DC} \cdot V_{Barrier} + \gamma_{LL} \cdot V_{LL} = 86.825\ kip$ — Postcomposite Factored Shear

$V_{uPre} := \gamma_{DC} \cdot V_{Pre} = 30.663\ kip$ Precomposite Factored Shear

$q_u := \frac{V_u \cdot Q_{Post}}{I_{transPost} \cdot n_{stud}} + \frac{V_{uPre} \cdot Q_{Pre}}{I_{transPre} \cdot n_{stud}} = 2.486\ \frac{kip}{in}$ Factored Shear Flow

## Fatigue I Shear Loading

$\gamma_{LL} := 1.75$ $IM := 1.15$
$\gamma_{DW} := 1.0$ $\gamma_{DC} := 1.0$ Load and Impact Factors

$g_v := 0.5$ Shear Distribution Factor

$P := 32\ kip$ Fatigue Truck Axle Load
$s := 30\ ft$ Fatigue Truck Axle Spacing
$a := 0\ ft$
$b := L - (a + s) = 23\ ft$

$V_{truck} := \frac{P}{L} \cdot (L - a + b) = 45.887\ kip$ Fatigue Truck Shear

$\gamma V_{Fatigue} := \gamma_{LL} \cdot IM \cdot V_{truck} \cdot g_v = 46.174\ kip$ Factored Fatigue Shear

$\gamma V_{DeadPre} := \gamma_{DC} \cdot V_{Pre}$

$\gamma V_{DeadPost} := \gamma_{DW} \cdot V_{ws} + \gamma_{DC} \cdot V_{Barrier} = 2.36\ kip$ Factored Dead Load Shear

$q_{Live} := \frac{\gamma V_{Fatigue} \cdot Q_{Post}}{I_{transPost} \cdot n_{stud}} = 0.918\ \frac{kip}{in}$ Factored Live Load Shear Flow

$q_{DeadPre} := \frac{\gamma V_{DeadPre} \cdot Q_{Pre}}{I_{transPre} \cdot n_{stud}} = 0.608\ \frac{kip}{in}$ Factored Dead Load Shear Flow

$q_{DeadPost} := \frac{\gamma V_{DeadPost} \cdot Q_{Post}}{I_{transPost} \cdot n_{stud}} = 0.047\ \frac{kip}{in}$

$q_{Dead} := q_{DeadPre} + q_{DeadPost} = 0.654\ \frac{kip}{in}$

## Fatigue Loads for Ridged Push-Out Specimens

| | |
|---|---|
| $n := 2$ | Number of GFRP Plates |
| $l := 22\ in$ | Length of Contact between Plates and Concrete |
| $P_{range} := n \cdot l \cdot q_{Live} = 40.403\ kip$ | Load Range to Apply Fatigue Live Load Shear Flow |
| $P_{dead} := n \cdot l \cdot (q_{DeadPre} + q_{DeadPost}) = 28.797\ kip$ | Load to Apply Fatigue Dead Load Shear Flow |
| $P_{min} := \max(P_{dead}, 10\ kip) = 28.797\ kip$ | Minimum Applied Test Load |
| $P_{max} := P_{min} + P_{range} = 69.201\ kip$ | Maximum Applied Test Load |
| $P_{mid} := \frac{P_{range}}{2} + P_{min} = 48.999\ kip$ | Average Applied Test Load |

$q_u = 2.49\ \frac{kip}{in}$

$q_{Live} = 0.92\ \frac{kip}{in}$

$q_{Dead} = 0.65\ \frac{kip}{in}$

$P_{min} = 28.8\ kip$

$P_{max} = 69.2\ kip$

$P_{mid} = 49\ kip$


Transportation Infrastructure Durability Center
AT THE UNIVERSITY OF MAINE

35 Flagstaff Road
Orono, Maine 04469
tidc@maine.edu
207.581.4376

**www.tidc-utc.org**